European Journal of Mechanics / A Solids 119 (2026) 106147

Contents lists available at ScienceDirect

European Journal of Mechanics / A Solids

journal homepage: www.elsevier.com/locate/ejmsol

Full length article

A functionally graded beam model accounting for thickness stretch

Davide Pellecchia [a,*], Francesco Marmo [a], Giambattista Romano [a], Eugenio Ruocco [b]

[a] *Department of Structures for Engineering and Architecture, University of Naples Federico II, via Claudio 21, 80125 Naples, Italy*
[b] *Department of Engineering, University of Campania Luigi Vanvitelli, via Roma 28, 81031 Aversa (Ce), Italy*

ARTICLE INFO

Keywords:
Functionally graded material
FGM
Functionally graded beam
Reddy beam model
Third-order shear deformation theory
Poisson effect
Thickness stretch
Finite element method
FEM

ABSTRACT

This paper presents an enhanced Reddy-type beam formulation for functionally graded materials, in which the mechanical properties vary continuously through the beam thickness. The proposed model extends the classical third-order shear deformation Reddy beam by introducing additional kinematic fields that allow for the transverse contractions and expansions of the beam cross section. The governing equations are derived in a variational form, from which the energetically conjugate generalised stresses, distributed loads and concentrated forces are consistently defined. The constitutive model for functionally graded materials is formulated by deriving analytical expressions for the entries of the local stiffness tensor, i.e. the higher-order elastic moments, employing an arbitrary polynomial variation of the Young modulus along the beam thickness. The elastic equilibrium equations are consistently derived and the analysis of the functionally graded beam is conducted by formulating a one-dimensional two-node finite element, with linear and cubic Hermite shape functions, for which the displacement and strain operators are explicitly derived and expressed in matrix form. Numerical investigations are carried out on both homogeneous and functionally graded beams. The proposed beam model successfully reproduces the nonlinear stress distributions along the thickness associated with the enriched kinematics and accurately captures localised boundary effects induced by external loads and constraints, yielding a richer and more physically consistent stress state compared to conventional beam models. Comparisons with two-dimensional continuum finite element analyses and benchmark results from the literature confirm the accuracy, robustness and predictive capabilities of the proposed model.

1. Introduction

Functionally graded materials (FGMs) are a class of advanced composite materials characterised by a smooth and continuous spatial variation of their microstructure and of their mechanical properties along one or more directions. Originally conceived in Japan in the 1980s to mitigate delamination problems in thermal barrier coatings for rocket engines (Hirai and Chen, 1999), FGMs have since evolved into a versatile solution for a wide range of structural applications.

The continuous variation of material properties along a preferred direction, which characterises FGMs, eliminates the abrupt material interfaces that are typical of laminated composites, thereby significantly reducing interfacial stress concentrations and enhancing structural integrity (Jin et al., 2019). This smooth gradation enables the tailoring of the material response during the design stage, allowing engineers to achieve desired distributions of stiffness, strength, thermal conductivity or even acoustic impedance within a single continuous medium (Chen et al., 2025).

Such unique characteristics make FGMs attractive for modern engineering systems that demand both structural performance and functional adaptability. In recent years, FGMs have found widespread applications as load-bearing or protective components across several fields, including civil engineering (Zhang et al., 2025), automotive design (Woodward and Kashtalyan, 2012), aerospace structures (Van Huong et al., 2025; Shao et al., 2025) and defence technologies (Zhang and Yuan, 2025; Liu et al., 2025). For instance, bamboo-inspired graded aluminum foams have demonstrated remarkable improvements in mechanical strength and thermal insulation (Zhang et al., 2025), while FGM-based aerospace panels and shells have exhibited superior thermal stability, vibration performance and impact resistance (Van Huong et al., 2025; Shao et al., 2025; Zhang and Yuan, 2025).

The mechanical behaviour of functionally graded beams has been extensively investigated over the past decades through various theories that can be generally classified into three main categories. The classical beam theory (CBT), also known as the Euler–Bernoulli beam theory, assumes

* Corresponding author.
E-mail address: davide.pellecchia@unina.it (D. Pellecchia).

https://doi.org/10.1016/j.euromechsol.2026.106147
Received 20 January 2026; Received in revised form 25 March 2026; Accepted 6 April 2026
Available online 12 April 2026

that plane cross sections normal to the mid-plane before deformation remain plane and normal after deformation (Love, 2013). Although simple, this beam theory becomes inaccurate for thick beams, as the model neglects transverse shear deformation. To address this limitation, the first-order shear deformation theory (FSDT), commonly referred to as the Timoshenko beam theory, was introduced to account for shear deformation. However, in the FSDT, the transverse shear stress through the beam thickness is only represented as a constant. To account for the inaccuracy in predicting the transverse shear force magnitude, and not to correct the shear stress distribution itself to satisfy the stress-free boundary conditions, a shear correction factor must be introduced (Reddy, 2022).

To further enhance the accuracy, higher-order shear deformation theories (HSDTs) have been developed, in which the transverse shear stresses vary nonlinearly across the thickness without requiring shear correction factors (Ruocco and Reddy, 2023a). These models provide more realistic predictions of the beam kinematics and stress fields, particularly for moderately thick and functionally graded structures. Several analytical and numerical formulations have been proposed within in this context, employing classical solution techniques such as the Levy, Navier and Galerkin methods or finite element approaches. Notable examples include the trigonometric theories proposed by Touratier (1991), Nguyen et al. (2014) and Mantari et al. (2012); the hyperbolic models developed by Soldatos (1992), Mahi et al. (2015) and Grover et al. (2013); and the exponential shear deformation theory formulated by Karama et al. (2003). A unified formulation was later introduced by Carrera (2003) and further applied to FGM beams by Filippi et al. (2015). Among the various third-order theories, Reddy's variationally consistent third-order shear deformation model (Reddy, 1984; Heyliger and Reddy, 1988; Reddy, 2022) remains one of the most widely used in the literature due to its balance between accuracy and analytical tractability.

Early contributions mainly addressed the static and dynamic response of linear FG beams, considering both homogeneous and graded materials (Aydogdu and Taskin, 2007; Kadoli et al., 2008; Ying et al., 2008). Specifically, Aydogdu and Taskin (2007) employed the Timoshenko beam theory to perform free vibration analyses of FG beams with simply supported boundaries, highlighting the influence of shear deformation and material gradation on natural frequencies. Kadoli et al. (2008) adopted a higher-order shear deformation beam model to study the static bending response under mechanical loading, while Ying et al. (2008) provided exact two-dimensional elasticity solutions for FG beams resting on elastic foundations, offering benchmark results for assessing the accuracy of one-dimensional formulations.

In recent years, the FEM has proven to be a highly versatile tool and has been extensively applied to analyse the complex mechanical, dynamic and stability behaviour of advanced functionally graded, porous and nanocomposite structures under various loading and boundary conditions (Bousmaha et al., 2025; Meftah et al., 2024; Tounsi et al., 2026; Belabed et al., 2024b; Lakhdar et al., 2024; Youzera et al., 2025; Belabed et al., 2024a). Subsequent studies expanded the analysis to include temperature-dependent effects, general boundary conditions, nonlocal integral elasticity and variations of material properties along the beam thickness (Mahi et al., 2010; Murin et al., 2010; Vaccaro et al., 2022; Simsek, 2010).

Further contributions have compared the predictions of Euler–Bernoulli, Timoshenko and generalised Reddy-type theories, providing analytical or semi-analytical solutions for bending and vibration problems. For instance, the free vibration and buckling behaviour of FG Euler–Bernoulli columns subjected to axial compressive force have been analysed by Lee and Lee (2019). Pradhan and Chakraverty (2013) have investigated the free vibration behaviour of Euler–Bernoulli and Timoshenko FG beams by means of the Rayleigh–Ritz method, offering reference results for a wide range of boundary conditions. Fu et al. (2013) have examined the thermal buckling response of FG beams containing longitudinal cracks, highlighting the sensitivity of critical loads to the material gradation and crack depth. Li and Batra (2013) have established analytical relations between the buckling loads of FG Timoshenko and homogeneous Euler–Bernoulli beams, while Li et al. (2013) have derived closed-form bending solutions for FG Timoshenko beams from those of homogeneous counterparts, thus providing useful transformation formulas between different beam models. Ruocco et al. (2021) and Ruocco and Reddy (2022) have proposed a homogeneous five-parameter Timoshenko beam model to capture linear and nonlinear behaviour and Poisson-induced coupling mechanisms.

In the afore-cited papers, the effective material properties of FGMs are usually assumed to obey the Voigt model. Although the Voigt model has been adopted in most analyses of FGM structures (Shen, 2009), doubts remain regarding the accuracy of applying the Voigt model in bending, buckling and vibration analyses of structures made of FGMs (Shen and Wang, 2014).

Recently, Pellecchia et al. (2024) have derived analytical expressions for evaluating the inertia properties of functionally graded two-dimensional domains and axisymmetric solids along arbitrary directions. These solutions, obtained for polynomial, exponential and quadratic distributions of material properties, provide a general and flexible framework for the accurate computation of effective stiffness quantities. This analytical approach can be naturally extended to the case of functionally graded beams, allowing for the adoption of more general and physically consistent material gradations within the beam's cross section.

The main novelties and original contributions of the present paper can be summarised as follows: we extend and develop in a consistent manner the enriched version of the classical homogeneous Reddy beam model (Reddy, 2022; Ruocco et al., 2025) in which additional kinematic fields are taken into account for the thickness stretch of the beam cross section. Specifically, the model is here further extended by formulating the constitutive model for functionally graded materials by deriving analytical expressions for the local stiffness tensor and its higher-order elastic moments, allowing for an arbitrary polynomial variation of the Young modulus along the beam thickness. Indeed, the inclusion of the thickness stretching effect becomes physically important, thereby justifying the adoption of this enhanced formulation over classical or standard higher-order theories, for instance for thick FG structures (Carrera et al., 2011; Thai and Kim, 2013; Vo et al., 2015; Akavci and Tanrikulu, 2015) where, as noted by Reddy (2017) Sec. 2.5.3, classical beam theory solutions "are in error compared with the plane elasticity solution (primarily because of the Poisson effect)". Finally, accounting for thickness stretching is critical in the presence of localised loads and constrained boundaries, where complex localised 3D stress states arise, making the evaluation of the transverse normal strain essential.

In summary, the primary advantages of the proposed model are twofold. First, it systematically overcomes the kinematic limitations associated with an undeformable cross-section assumption, accurately predicting transverse normal stresses and capturing the Poisson effect without requiring ad-hoc correction factors. Second, compared to full 3D solid models, this variationally consistent 1D formulation drastically reduces the computational effort while maintaining a comparable level of accuracy in evaluating complex, localised stress fields in functionally graded structures.

The corresponding elastic equilibrium equations are derived in a consistent manner by employing variational principle. The analysis of the FG beam is carried out using the finite element method using a one-dimensional two-node element, with linear and cubic Hermite shape functions. The displacement and strain operators are explicitly derived and expressed in matrix form, ensuring full compatibility with the variational formulation.

A comprehensive numerical assessment is carried out on both homogeneous and FG beams. The proposed model accurately reproduces the nonlinear stress distributions associated with material gradation and successfully captures local boundary effects induced by external loads and

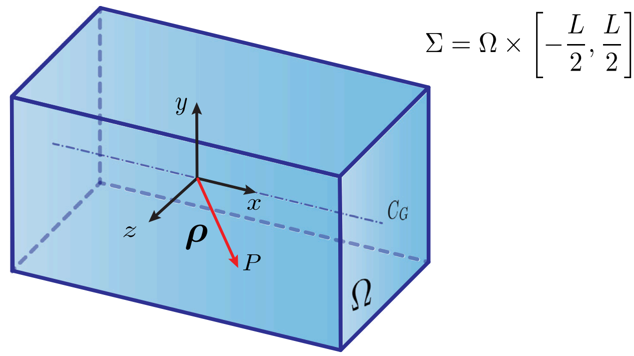

Fig. 1. Geometry of the Reddy beam model of length L having rectangular cross section. The three-dimensional solid domain is denoted by Σ, while Ω represents the two-dimensional cross section domain. The position vector ρ identifies a generic point P within the beam. The geometric centroid of the cross section is indicated by C_G.

constraints, resulting in a richer and more physically consistent stress field compared to conventional beam models. Comparisons with two-dimensional continuum finite element analyses and benchmark results from the literature (Li et al., 2019; Ruocco and Reddy, 2023b; Müsevitoğlu et al., 2025) confirm the accuracy, robustness and predictive capability of the proposed formulation.

From a practical engineering standpoint, the proposed model provides a computationally efficient and accurate tool for the design and structural optimisation of advanced FGM components. Typical practical applications include aerospace engineering, e.g., thermal protection systems and rocket engine components and naval architecture.

The paper is organised as follows. A brief overview of the geometry and kinematic equations of the classical Reddy beam is presented in Section 2. Subsequently, the enriched kinematics of the enhanced Reddy beam model is shown in Section 3, where the local equilibrium equations and their corresponding boundary conditions are derived in a variationally consistent form. In Section 4, the constitutive equations for FGMs are formulated and analytical expressions are derived for the entries of the local stiffness tensor. Section 5 presents the derivation of the elastic equilibrium equations, while Section 6 details their finite element formulation based on one-dimensional beam elements. Lastly, Section 7 discusses several numerical examples illustrating the performance and accuracy of the proposed formulation while the main conclusions are summarised in Section 8.

2. Geometry and kinematics of the classical Reddy beam model

Let ρ be the position vector that identifies an arbitrary point P within the three-dimensional beam model having the shape of a right prism of length L with a rectangular cross section modelled as a two-dimensional domain Ω. The overall domain of the solid is defined as $\Sigma = \Omega\times\left[-\frac{L}{2}, \frac{L}{2}\right]$. A Cartesian reference frame is adopted such that the x-axis, oriented along the longitudinal axis of the beam, is centred at the midspan and coincides with the locus of the geometric centroids of the cross sections, while the y- and z-axes belong to the cross section, see Fig. 1. The displacements vector field of the Reddy third-order beam $\mathbf{u}^R(\rho)$ reads (Heyliger and Reddy, 1988)

$$[\mathbf{u}^R(\rho)] = \begin{bmatrix} u_x^R(\rho) \\ u_y^R(\rho) \\ u_z^R(\rho) \end{bmatrix} = \begin{bmatrix} w(x) - y\,\phi(x) + y^2\,\zeta(x) + y^3\,\lambda(x) \\ v(x) \\ 0 \end{bmatrix}, \tag{1}$$

where $w(x)$ and $v(x)$ are the cross section displacements along the x and y-axes, respectively, while $\phi(x)$, $\zeta(x)$ and $\lambda(x)$ are defined as

$$\phi(x) = -\partial_y\,(u_x^R)\Big|_{y=0}, \qquad \zeta(x) = \frac{1}{2!}\,\partial_y^2\,(u_x^R)\Big|_{y=0} \qquad \text{and} \qquad \lambda(x) = \frac{1}{3!}\,\partial_y^3\,(u_x^R)\Big|_{y=0}, \tag{2}$$

in which $\partial_j^n(\bullet) = \partial^n(\bullet)/\partial j^n$. Notice that the displacement component $u_z^R(\rho)$ in Eq. (1) is constrained to be zero in order to prevent bending in the $x-z$ plane.

The components of the infinitesimal strain tensor are obtained by invoking kinematic compatibility of the displacements field providing

$$[\varepsilon^R(\rho)] = \begin{bmatrix} \varepsilon_x^R(\rho) \\ \varepsilon_y^R(\rho) \\ \gamma_{yx}^R(\rho) \end{bmatrix} = \begin{bmatrix} w'(x) - y\,\phi'(x) + y^2\,\zeta'(x) + y^3\,\lambda'(x) \\ 0 \\ v'(x) - \phi(x) + 2\,y\,\zeta(x) + 3\,y^2\,\lambda(x) \end{bmatrix}, \tag{3}$$

where $(\bullet)'$ $[(\bullet)'']$ stands for first [second] derivative along the x-axis.

The quantities scaling the quadratic and cubic terms of $u_x^R(\rho)$ in Eq. (1), namely $\zeta(x)$ and $\lambda(x)$, are obtained by imposing the vanishing of shear strain at the top and bottom surfaces of the beam, i.e. $\gamma_{xy}^R(\pm h/2) = 0$, with h the height of the cross section, yielding

$$\zeta(x) = 0 \qquad \text{and} \qquad \lambda(x) = \alpha\,\big(\phi(x) - v'(x)\big), \tag{4}$$

where $\alpha = 4/(3\,h^2)$. Hence, enforcing the vanishing of the shear strain at the top and bottom surfaces of the cross section reduces the number of unknowns, since the variable $\zeta(x)$ disappears while $\lambda(x)$ is expressed as function of $\phi(x)$ and $v'(x)$.

Consequently, unlike the Timoshenko beam theory that assumes a uniform shear strain distribution and thus requires the introduction of a shear correction factor, the third-order beam theory captures the correct shear strain profile, eliminating the need for such correction factor.

The displacements field (1) can be rewritten in the following way

$$[\mathbf{u}^R(\rho)] = \begin{bmatrix} w(x) - y\,\phi(x) + y^3\,\alpha\,\big(\phi(x) - v'(x)\big) \\ v(x) \\ 0 \end{bmatrix}, \tag{5}$$

and the strains field (3) as

$$[\varepsilon^R(\rho)] = \begin{bmatrix} w'(x) - y\,\phi'(x) + y^3\,\alpha\,\big(\phi'(x) - v''(x)\big) \\ 0 \\ (\beta\,y^2 - 1)\,\big(\phi(x) - v'(x)\big) \end{bmatrix}, \tag{6}$$

where $\beta = 3\,\alpha$.

In the next Section, we introduce a novel third-order beam theory derived from the classical Reddy beam model, featuring an enriched kinematics capable of accounting for thickness stretch.

3. Kinematics and equilibrium equations of the proposed third-order beam model

In order to account for thickness stretch, the kinematics of the proposed model is obtained by supplementing the displacement field $\mathbf{u}^R(\rho)$ considered in the previous Section with two further addends

$$[\mathbf{u}(\rho)] = \begin{bmatrix} u_x(\rho) \\ u_y(\rho) \\ u_z(\rho) \end{bmatrix} = \begin{bmatrix} w(x) - y\,\phi(x) + y^2\,\zeta(x) + y^3\,\lambda(x) \\ v(x) + y\,\theta(x) + y^2\,\psi(x) \\ 0 \end{bmatrix}. \tag{7}$$

Specifically, the linear and quadratic terms defined as

$$\theta(x) = \partial_y\,(u_y)\Big|_{y=0} \qquad \text{and} \qquad \psi(x) = \frac{1}{2!}\,\partial_y^2\,(u_y)\Big|_{y=0}, \tag{8}$$

are responsible for the stretching of the beam cross section, thus allowing for expansion or contraction along the y-axis.

Hence, the components of the infinitesimal shear strain based on the displacement field in Eq. (7) are given by

$$[\varepsilon(\rho)] = \begin{bmatrix} \varepsilon_x(\rho) \\ \varepsilon_y(\rho) \\ \gamma_{yx}(\rho) \end{bmatrix} = \begin{bmatrix} w'(x) - y\,\phi'(x) + y^2\,\zeta'(x) + y^3\,\lambda'(x) \\ \theta(x) + 2\,y\,\psi(x) \\ \big(v'(x) - \phi(x)\big) + y\,\big(2\,\zeta(x) + \theta'(x)\big) + y^2\,\big(3\,\lambda(x) + \psi'(x)\big) \end{bmatrix}. \tag{9}$$

Analogously to the classical Reddy beam model, the parameters $\zeta(x)$ and $\lambda(x)$ are obtained by imposing the vanishing of the shear strain γ_{yx} at the boundary of the beam cross section; this yields

$$\zeta(x) = -\frac{\theta'(x)}{2} \qquad \text{and} \qquad \lambda(x) = \alpha\,\big(\phi(x) - v'(x)\big) - \frac{\psi'(x)}{3}. \tag{10}$$

so that, the displacement field (7) becomes

$$[\mathbf{u}(\rho)] = \begin{bmatrix} w(x) - y\,\phi(x) - y^2\,\dfrac{\theta'(x)}{2} + y^3\left(\alpha\left(\phi(x) - v'(x)\right) - \dfrac{\psi'(x)}{3}\right) \\ v(x) + y\,\theta(x) + y^2\,\psi(x) \\ 0 \end{bmatrix}. \tag{11}$$

By specialising the strain field (9) as

$$[\varepsilon(\rho)] = \begin{bmatrix} w'(x) - y\,\phi'(x) - y^2\,\dfrac{\theta''(x)}{2} + y^3\left[\alpha\left(\phi'(x) - v''(x)\right) - \dfrac{\psi''(x)}{3}\right] \\ \theta(x) + 2\,y\,\psi(x) \\ (\beta\,y^2 - 1)\,\big(\phi(x) - v'(x)\big) \end{bmatrix}, \tag{12}$$

and comparing it with that associated with the Reddy beam model in Eq. (6), we notice that the axial strain ε_x is enriched with new additional terms while ε_y is no longer zero. Conversely, γ_{yx} remains the same for the two models, as the terms $\theta'(x)$ and $\psi'(x)$ exactly cancel out upon enforcing the zero-shear-strain boundary conditions at the top and bottom surfaces.

3.1. Derivation of the local equilibrium equations by variational principle

The local equilibrium equations and the associated boundary conditions are derived by invoking the variational equilibrium condition. To this end, we first establish the expressions for the internal and external work.

Assuming plane stress at each point of the beam, i.e.

$$\sigma_z(\rho) = \tau_{xz}(\rho) = \tau_{yz}(\rho) = 0, \tag{13}$$

the non-zero components of the Cauchy stress tensor can be collected in a vector, e.g. $[\sigma(\rho)] = [\sigma_x(\rho), \sigma_y(\rho), \tau_{yx}(\rho)]^T$.

The internal work

$$W_I = \int_{-\frac{L}{2}}^{\frac{L}{2}} \int_{\Omega} \sigma_x(\rho)\,\varepsilon_x(\rho)\,\mathrm{d}A\,\mathrm{d}x + \int_{-\frac{L}{2}}^{\frac{L}{2}} \int_{\Omega} \sigma_y(\rho)\,\varepsilon_y(\rho)\,\mathrm{d}A\,\mathrm{d}x + \int_{-\frac{L}{2}}^{\frac{L}{2}} \int_{\Omega} \tau_{yx}(\rho)\,\gamma_{yx}(\rho)\,\mathrm{d}A\,\mathrm{d}x \tag{14}$$

can be rewritten by expressing the strain components as function of the generalised displacement components of Eq. (12), furnishing

$$
\begin{aligned}
W_I = &\int_{-\frac{L}{2}}^{\frac{L}{2}} \int_{\Omega} \sigma_x(\rho)\, \mathrm{d}A\, w'(x)\, \mathrm{d}x + \int_{-\frac{L}{2}}^{\frac{L}{2}} \int_{\Omega} -\sigma_x(\rho)\, y\, \mathrm{d}A\, \phi'(x)\, \mathrm{d}x + \int_{-\frac{L}{2}}^{\frac{L}{2}} \int_{\Omega} -\sigma_x(\rho)\, y^2\, \mathrm{d}A\, \frac{\theta''(x)}{2}\, \mathrm{d}x \\
&+ \int_{-\frac{L}{2}}^{\frac{L}{2}} \int_{\Omega} \sigma_x(\rho)\, y^3\, \mathrm{d}A \left[\alpha \left(\phi'(x) - v''(x)\right) - \frac{\psi''(x)}{3}\right] \mathrm{d}x \\
&+ \int_{-\frac{L}{2}}^{\frac{L}{2}} \int_{\Omega} \sigma_y(\rho)\, \mathrm{d}A\, \theta(x)\, \mathrm{d}x + \int_{-\frac{L}{2}}^{\frac{L}{2}} \int_{\Omega} \sigma_y(\rho)\, y\, \mathrm{d}A\, 2\, \psi(x)\, \mathrm{d}x \\
&+ \int_{-\frac{L}{2}}^{\frac{L}{2}} \int_{\Omega} -\tau_{yx}(\rho)\, \mathrm{d}A \left(\phi(x) - v'(x)\right) \mathrm{d}x + \int_{-\frac{L}{2}}^{\frac{L}{2}} \int_{\Omega} \tau_{yx}(\rho)\, y^2\, \mathrm{d}A\, \beta \left(\phi(x) - v'(x)\right) \mathrm{d}x.
\end{aligned} \tag{15}
$$

It is worth noting that the collection of the generalised displacement components in Eq. (15) is in accordance with the classical definitions of generalised strain and stress resultants in Euler–Bernoulli and Timoshenko beam theories. Specifically, each term in the internal work expression corresponds to the product of a section-level strain, i.e. axial strain, bending strain and shear strain, and the associated stress resultant, i.e. the integral of the stress distribution along the thickness coordinate y. This consistency underscores how the enhanced Reddy model naturally extends these classical and first-order beam theories while preserving their fundamental variational structure.

Hence, the resultant stresses and their kinematic duals may be stored in the following two vectors

$$
[\boldsymbol{\sigma}_{\Omega}(x)] = \int_{\Omega} \begin{bmatrix} \sigma_x(\rho) \\ \sigma_x(\rho)\, y \\ \sigma_x(\rho)\, y^2 \\ \sigma_x(\rho)\, y^3 \\ \sigma_y(\rho) \\ \sigma_y(\rho)\, y \\ \tau_{yx}(\rho) \\ \tau_{yx}(\rho)\, y^2 \end{bmatrix} \mathrm{d}A = \begin{bmatrix} M_0(x) \\ -M_1(x) \\ -M_2(x) \\ M_3(x) \\ \hat{M}_0(x) \\ \hat{M}_1(x) \\ -T_0(x) \\ T_2(x) \end{bmatrix}, \quad [\boldsymbol{\varepsilon}_{\Omega}(x)] = \begin{bmatrix} w'(x) \\ \phi'(x) \\ \dfrac{\theta''(x)}{2} \\ \alpha \left(\phi'(x) - v''(x)\right) - \dfrac{\psi''(x)}{3} \\ \theta(x) \\ 2\, \psi(x) \\ \phi(x) - v'(x) \\ \beta\, (\phi(x) - v'(x)) \end{bmatrix} = \begin{bmatrix} \varepsilon_0(x) \\ \varepsilon_1(x) \\ \varepsilon_2(x) \\ \varepsilon_3(x) \\ \hat{\varepsilon}_0(x) \\ \hat{\varepsilon}_1(x) \\ \gamma_0(x) \\ \gamma_2(x) \end{bmatrix}, \tag{16}
$$

where $\boldsymbol{\sigma}_{\Omega}(x)$ and $\boldsymbol{\varepsilon}_{\Omega}(x)$ are the vectors of the generalised stress and strain, respectively.

Among these, M_0, M_1 and T_0 correspond to the classical Timoshenko stress resultants, namely the axial force, bending moment and shear force, associated with the axial strain ε_0, bending curvature ε_1 and shear strain γ_0, respectively. The additional resultants M_2, M_3, $\hat{M}_0$, $\hat{M}_1$ and T_2, together with their kinematic duals, are novel contributions introduced by the present model. These arise from the enriched kinematics and the inclusion of the transverse normal stress σ_y, which is typically neglected in the classical Reddy theory (Reddy, 2017).

Employing integration by parts in Eq. (15) and collecting the coefficients of the generalised displacements as well as $v'(x)$, $\theta'(x)$ and $\psi'(x)$, we obtain

$$
\begin{aligned}
W_I = &- \int_{-\frac{L}{2}}^{\frac{L}{2}} M_0'(x)\, w(x)\, \mathrm{d}x + M_0(x)\, w(x) \Big|_{-\frac{L}{2}}^{\frac{L}{2}} \\
&- \int_{-\frac{L}{2}}^{\frac{L}{2}} \left(\alpha\, M_3''(x) + T_0'(x) - \beta\, T_2'(x)\right) v(x)\, \mathrm{d}x + \left(\alpha\, M_3'(x) + T_0(x) - \beta\, T_2(x)\right) v(x) \Big|_{-\frac{L}{2}}^{\frac{L}{2}} \\
&+ \int_{-\frac{L}{2}}^{\frac{L}{2}} \left(M_1'(x) - \alpha\, M_3'(x) - T_0(x) + \beta\, T_2(x)\right) \phi(x)\, \mathrm{d}x + \left(-M_1(x) + \alpha\, M_3(x)\right) \phi(x) \Big|_{-\frac{L}{2}}^{\frac{L}{2}} \\
&+ \int_{-\frac{L}{2}}^{\frac{L}{2}} \left(-\frac{M_2''(x)}{2} + \hat{M}_0(x)\right) \theta(x)\, \mathrm{d}x + \frac{M_2'(x)}{2}\, \theta(x) \Big|_{-\frac{L}{2}}^{\frac{L}{2}} - \int_{-\frac{L}{2}}^{\frac{L}{2}} \left(\frac{M_3''(x)}{3} - 2\, \hat{M}_1(x)\right) \psi(x)\, \mathrm{d}x + \frac{M_3'(x_i)}{3}\, \psi(x) \Big|_{-\frac{L}{2}}^{\frac{L}{2}} \\
&- \alpha\, M_3(x)\, v'(x) \Big|_{-\frac{L}{2}}^{\frac{L}{2}} - \frac{M_2(x)}{2}\, \theta'(x) \Big|_{-\frac{L}{2}}^{\frac{L}{2}} - \frac{M_3(x)}{3}\, \psi'(x) \Big|_{-\frac{L}{2}}^{\frac{L}{2}}.
\end{aligned} \tag{17}
$$

The expression of the external work is obtained by first defining the concentrated forces $\mathscr{F}_w$, $\mathscr{F}_v$, $\mathscr{F}_\phi$, $\mathscr{F}_\theta$, $\mathscr{F}_\psi$, $\mathscr{F}_{v'}$, $\mathscr{F}_{\theta'}$ and $\mathscr{F}_{\psi'}$ of the proposed model derived upon examining the boundary terms in Eq. (17). The subscripts of those forces identify the relevant duality pairs of the kinematic parameters.

Furthermore, let $q_w(x)$, $q_v(x)$, $q_\phi(x)$, $q_\theta(x)$ and $q_\psi(x)$ be the distributed loads associated with the generalised displacement field. Finally, the external work is given by

$$
\begin{aligned}
W_E = &\int_{-\frac{L}{2}}^{\frac{L}{2}} q_w(x)\, w(x)\, \mathrm{d}x + \int_{-\frac{L}{2}}^{\frac{L}{2}} q_v(x)\, v(x)\, \mathrm{d}x + \int_{-\frac{L}{2}}^{\frac{L}{2}} q_\phi(x)\, \phi(x)\, \mathrm{d}x + \int_{-\frac{L}{2}}^{\frac{L}{2}} q_\theta(x)\, \theta(x)\, \mathrm{d}x + \int_{-\frac{L}{2}}^{\frac{L}{2}} q_\psi(x)\, \psi(x)\, \mathrm{d}x \\
&+ \mathscr{F}_w(x_i)\, w(x_i) + \mathscr{F}_v(x_i)\, v(x_i) + \mathscr{F}_\phi(x_i)\, \phi(x_i) + \mathscr{F}_\theta(x_i)\, \theta(x_i) + \mathscr{F}_\psi(x_i)\, \psi(x_i) + \mathscr{F}_{v'}(x_i)\, v'(x_i) + \mathscr{F}_{\theta'}(x_i)\, \theta'(x_i) + \mathscr{F}_{\psi'}(x_i)\, \psi'(x_i),
\end{aligned} \tag{18}
$$

where $i = \{1, 2\}$ with $x_1 = -L/2$, $x_2 = L/2$.

Therefore, using the variational equilibrium condition and the fundamental lemma of the calculus of variations, we obtain the following local equilibrium equations

$$M_0'(x) + q_w(x) = 0, \tag{19a}$$

$$\alpha\, M_3''(x) + T_0'(x) - \beta\, T_2'(x) + q_v(x) = 0, \tag{19b}$$

$$M_1'(x) - \alpha\, M_3'(x) - T_0(x) + \beta\, T_2(x) - q_\phi(x) = 0, \tag{19c}$$

$$\frac{M_2''(x)}{2} - \hat{M}_0(x) + q_\theta(x) = 0, \tag{19d}$$

$$-\frac{M_3''(x)}{3} + 2\,\hat{M}_1(x) - q_\psi(x) = 0, \tag{19e}$$

equipped with the following boundary conditions

$$M_0(x_i) = n_i\, \mathscr{F}_w(x_i), \tag{20a}$$

$$\alpha\, M_3'(x_i) + T_0(x_i) - \beta\, T_2(x_i) = n_i\, \mathscr{F}_v(x_i), \tag{20b}$$

$$-M_1(x_i) + \alpha\, M_3(x_i) = n_i\, \mathscr{F}_\phi(x_i), \tag{20c}$$

$$\frac{M_2'(x_i)}{2} = n_i\, \mathscr{F}_\theta(x_i), \tag{20d}$$

$$\frac{M_3'(x_i)}{3} = n_i\, \mathscr{F}_\psi(x_i), \tag{20e}$$

$$-\alpha\, M_3(x_i) = n_i\, \mathscr{F}_{v'}(x_i), \tag{20f}$$

$$-\frac{M_2(x_i)}{2} = n_i\, \mathscr{F}_{\theta'}(x_i), \tag{20g}$$

$$-\frac{M_3(x_i)}{3} = n_i\, \mathscr{F}_{\psi'}(x_i), \tag{20h}$$

where $n_1 = -1$, $n_2 = 1$.

4. Constitutive equations for linear elasticity and functionally graded Young modulus

We assume that the beam is composed of a functionally graded material (FGM) characterised by a Young modulus E that varies along the cross section thickness, identified by the y-axis, according to the following polynomial relationship (Shen, 2009):

$$E(y) = \sum_{q=0}^{m} E_q\, y^q, \tag{21}$$

where $E_0,\ E_1,\ \ldots,\ E_m$ are real coefficients and m is a non-negative integer. The assumption that the Young's modulus varies solely along the y-direction, i.e., across the thickness of the beam cross section, ensures that the bending of the beam is constrained to the x–y plane, preventing bending in the $x - z$ plane.

It should be noted that the chosen functional form for the Young modulus is completely general, as many continuous functions can be very well approximated by a polynomial expansion.

Hence, the constitutive relation between the stress and strain fields for an isotropic and linear elastic material, reads

$$\boldsymbol{\sigma}(\boldsymbol{\rho}) = \mathbf{C}(y)\, \boldsymbol{\varepsilon}(\boldsymbol{\rho}), \tag{22}$$

being $\mathbf{C}(y)$ the elasticity tensor for plane stress state. Specifically, setting $\bar{E}(y) = E(y)/(1-\nu^2)$ and $G(y) = E(y)/[2\,(1+\nu)]$, one has

$$[\mathbf{C}(y)] = \begin{bmatrix} \bar{E}(y) & \nu\, \bar{E}(y) & 0 \\ \nu\, \bar{E}(y) & \bar{E}(y) & 0 \\ 0 & 0 & G(y) \end{bmatrix}, \tag{23}$$

where ν is the Poisson's ratio assumed to be a constant for the FGM.

Expressing the infinitesimal strains field $\boldsymbol{\varepsilon}(\boldsymbol{\rho})$ as a function of the generalised strain components $\boldsymbol{\varepsilon}_\Omega(x)$, one has

$$\boldsymbol{\varepsilon}(\boldsymbol{\rho}) = \mathbf{E}(y)\, \boldsymbol{\varepsilon}_\Omega(x), \tag{24}$$

where, based on Eq. (12), the matrix representation of $\mathbf{E}$ is

$$[\mathbf{E}(y)] = \begin{bmatrix} 1 & -y & -y^2 & y^3 & 0 & 0 & 0 & 0 \\ 0 & 0 & 0 & 0 & 1 & y & 0 & 0 \\ 0 & 0 & 0 & 0 & 0 & 0 & -1 & y^2 \end{bmatrix}. \tag{25}$$

Hence, by virtue of Eqs. (22) and (24), the internal work is amenable to the following equivalent form

$$\begin{aligned} W_I &= \int_{-\frac{L}{2}}^{\frac{L}{2}} \int_\Omega \boldsymbol{\sigma}(\boldsymbol{\rho}) \cdot \boldsymbol{\varepsilon}(\boldsymbol{\rho})\, \mathrm{d}A\, \mathrm{d}x = \int_{-\frac{L}{2}}^{\frac{L}{2}} \int_\Omega \mathbf{E}^T(y)\, \mathbf{C}(y)\, \mathbf{E}(y)\, \mathrm{d}A\, \boldsymbol{\varepsilon}_\Omega(x) \cdot \boldsymbol{\varepsilon}_\Omega(x)\, \mathrm{d}x \\ &= \int_{-\frac{L}{2}}^{\frac{L}{2}} \mathbf{K}_\Omega(x)\, \boldsymbol{\varepsilon}_\Omega(x) \cdot \boldsymbol{\varepsilon}_\Omega(x)\, \mathrm{d}x, \end{aligned} \tag{26}$$

being $\mathbf{K}_\Omega$ the local stiffness tensor that establishes the relationship between the generalised stress components with the generalised strain ones by the following formula $\boldsymbol{\sigma}_\Omega(x) = \mathbf{K}_\Omega(x)\,\boldsymbol{\varepsilon}_\Omega(x)$. The matrix representation of the local stiffness tensor is the following

$$[\mathbf{K}_\Omega(x)] = \begin{bmatrix} J_{\bar{E}}^{(0)} & -J_{\bar{E}}^{(1)} & -J_{\bar{E}}^{(2)} & J_{\bar{E}}^{(3)} & \nu\, J_{\bar{E}}^{(0)} & \nu\, J_{\bar{E}}^{(1)} & 0 & 0 \\ -J_{\bar{E}}^{(1)} & J_{\bar{E}}^{(2)} & J_{\bar{E}}^{(3)} & -J_{\bar{E}}^{(4)} & -\nu\, J_{\bar{E}}^{(1)} & -\nu\, J_{\bar{E}}^{(2)} & 0 & 0 \\ -J_{\bar{E}}^{(2)} & J_{\bar{E}}^{(3)} & J_{\bar{E}}^{(4)} & -J_{\bar{E}}^{(5)} & -\nu\, J_{\bar{E}}^{(2)} & -\nu\, J_{\bar{E}}^{(3)} & 0 & 0 \\ J_{\bar{E}}^{(3)} & -J_{\bar{E}}^{(4)} & -J_{\bar{E}}^{(5)} & J_{\bar{E}}^{(6)} & \nu\, J_{\bar{E}}^{(3)} & \nu\, J_{\bar{E}}^{(4)} & 0 & 0 \\ \nu\, J_{\bar{E}}^{(0)} & -\nu\, J_{\bar{E}}^{(1)} & -\nu\, J_{\bar{E}}^{(2)} & \nu\, J_{\bar{E}}^{(3)} & J_{\bar{E}}^{(0)} & J_{\bar{E}}^{(1)} & 0 & 0 \\ \nu\, J_{\bar{E}}^{(1)} & -\nu\, J_{\bar{E}}^{(2)} & -\nu\, J_{\bar{E}}^{(3)} & \nu\, J_{\bar{E}}^{(4)} & J_{\bar{E}}^{(1)} & J_{\bar{E}}^{(2)} & 0 & 0 \\ 0 & 0 & 0 & 0 & 0 & 0 & J_G^{(0)} & -J_G^{(2)} \\ 0 & 0 & 0 & 0 & 0 & 0 & -J_G^{(2)} & J_G^{(4)} \end{bmatrix}, \tag{27}$$

where the entries of $\mathbf{K}_\Omega(x)$ are defined as

$$J_{\bar{E}}^{(k)} = \int_\Omega \bar{E}(y)\, y^k \,\mathrm{d}A \quad \text{and} \quad J_G^{(k)} = \int_\Omega G(y)\, y^k \,\mathrm{d}A, \tag{28}$$

being the integer $k \geq 0$.

From a mechanical point of view, these entries represent characteristic quantities associated with both the cross section geometry and the material properties.

4.1. Analytical evaluation of the entries of the local stiffness tensor

Given a rectangular cross section having width b, the integrals (28) specialise as follows

$$J_{\bar{E}}^{(k)} = \frac{1}{1-\nu^2}\, J_E^{(k)} \quad \text{and} \quad J_G^{(k)} = \frac{1}{2\,(1+\nu)}\, J_E^{(k)}, \tag{29}$$

where

$$J_E^{(k)} = b \int_{-\frac{h}{2}}^{\frac{h}{2}} E(y)\, y^k \,\mathrm{d}y, \tag{30}$$

is the k-order elastic moments of area.

Invoking Eq. (21), the k-order elastic moment is amenable to the following equivalent form

$$J_E^{(k)} = b \sum_{q=0}^{m} E_q \int_{-\frac{h}{2}}^{\frac{h}{2}} y^{k+q} \,\mathrm{d}y. \tag{31}$$

where E_q is defined in Eq. (21).

To provide an explicit expression of the previous integral, we express the function y^{k+q} as derivative of a suitable higher-order function so as to apply the fundamental theorem of calculus.

Accordingly, exploiting the following result

$$\partial_y \left(y^{k+q+1}\right) = (k+q+1)\, y^{k+q}, \tag{32}$$

the integral (31) turns out to be

$$J_E^{(k)} = b \sum_{q=0}^{m} \frac{E_q}{k+q+1} \int_{-\frac{h}{2}}^{\frac{h}{2}} \partial_y \left(y^{k+q+1}\right) \mathrm{d}y = b \sum_{q=0}^{m} \frac{E_q}{k+q+1}\, y^{k+q+1}\Big|_{-\frac{h}{2}}^{\frac{h}{2}}, \tag{33}$$

where

$$y^{q+k+1}\Big|_{-\frac{h}{2}}^{\frac{h}{2}} = \begin{cases} 0, & \text{if } k+q+1 \text{ is even}, \\ h^{k+q+1}\, 2^{-(k+q)}, & \text{if } k+q+1 \text{ is odd}. \end{cases} \tag{34}$$

For completeness, we specialise the integral (33) for the case of $k = 0,\ 1,\ 2$, obtaining

$$\begin{aligned} J_E^{(0)} &= b \sum_{q=0}^{m} \frac{E_q}{q+1}\, y^{q+1}\Big|_{-\frac{h}{2}}^{\frac{h}{2}}, \\ J_E^{(1)} &= b \sum_{q=0}^{m} \frac{E_q}{q+2}\, y^{q+2}\Big|_{-\frac{h}{2}}^{\frac{h}{2}}, \\ J_E^{(2)} &= b \sum_{q=0}^{m} \frac{E_q}{q+3}\, y^{q+3}\Big|_{-\frac{h}{2}}^{\frac{h}{2}}, \end{aligned} \tag{35}$$

that represent, respectively, the zeroth-, first- and second-order elastic moments of area of the cross section, weighted by the polynomial distribution of the Young's modulus $E(y)$. Their evaluation is fundamental in the formulation of the stiffness terms of the beam model, as they govern the mechanical response of the model.

5. Elastic equilibrium equations for functionally graded enhanced Reddy beam model having Poisson effect

Let us set the following functions, defined in terms of derivatives of the generalised displacement fields:

$$\begin{aligned}
\gamma^{(p)}(x) &= \phi^{(p)}(x) - v^{(p+1)}(x),\\
\delta^{(p)}(x) &= \alpha\,\gamma^{(p)}(x) - \frac{\psi^{(p+1)}(x)}{3},\\
\eta^{(p)}(x) &= w^{(p+1)}(x) + \nu\,\theta^{(p)}(x),\\
\eta^{*(p)}(x) &= \nu\,w^{(p+1)}(x) + \theta^{(p)}(x),\\
\xi^{(p)}(x) &= 2\,\nu\,\psi^{(p)}(x) - \phi^{(p+1)}(x),\\
\xi^{*(p)}(x) &= 2\,\psi^{(p)}(x) - \nu\,\phi^{(p+1)}(x),
\end{aligned} \tag{36}$$

being p the order of differentiation. The elastostatic formulation of the functionally graded enhanced Reddy beam model accounting for thickness stretch is presented in the following

$$J_{\bar{E}}^{(0)}\,\eta'(x) + J_{\bar{E}}^{(1)}\,\xi'(x) - \frac{1}{2}\,J_{\bar{E}}^{(2)}\,\theta'''(x) + J_{\bar{E}}^{(3)}\,\delta''(x) + q_w(x) = 0, \tag{37a}$$

$$\left(-J_G^{(0)} + 2\,\beta\,J_G^{(2)} - \beta^2\,J_G^{(4)}\right)\gamma'(x) + \alpha\left(J_{\bar{E}}^{(3)}\,\eta''(x) + J_{\bar{E}}^{(4)}\,\xi'(x) - \frac{1}{2}\,J_{\bar{E}}^{(5)}\,\theta''''(x) + J_{\bar{E}}^{(6)}\,\delta'''(x)\right) + q_v(x) = 0, \tag{37b}$$

$$\begin{aligned}
&\left(J_G^{(0)} - 2\,\beta\,J_G^{(2)} + \beta^2\,J_G^{(4)}\right)\gamma(x) + J_{\bar{E}}^{(1)}\,\eta'(x) + J_{\bar{E}}^{(2)}\,\xi'(x) - \frac{1}{2}\,J_{\bar{E}}^{(3)}\,\theta'''(x) + J_{\bar{E}}^{(4)}\,\delta''(x)\\
&-\alpha\left(J_{\bar{E}}^{(3)}\,\eta'(x) + J_{\bar{E}}^{(4)}\,\xi'(x) - \frac{1}{2}\,J_{\bar{E}}^{(5)}\,\theta'''(x) + J_{\bar{E}}^{(6)}\,\delta''(x)\right) - q_\phi(x) = 0,
\end{aligned} \tag{37c}$$

$$J_{\bar{E}}^{(0)}\,\eta^*(x) + J_{\bar{E}}^{(1)}\,\xi^*(x) - J_{\bar{E}}^{(2)}\left(\nu\,\theta''(x) + \frac{1}{2}\,w'''(x)\right) + \nu\,J_{\bar{E}}^{(3)}\,\delta'(x) - \frac{1}{2}\,J_{\bar{E}}^{(3)}\,\xi'(x) + \frac{1}{4}\,J_{\bar{E}}^{(4)}\,\theta''''(x) - \frac{1}{2}\,J_{\bar{E}}^{(5)}\,\delta'''(x) - q_\theta(x) = 0, \tag{37d}$$

$$2\,J_{\bar{E}}^{(1)}\,\eta^*(x) + 2\,J_{\bar{E}}^{(2)}\,\xi^*(x) - \nu\,J_{\bar{E}}^{(3)}\,\theta''(x) + 2\,\nu\,J_{\bar{E}}^{(4)}\,\delta'(x) - \frac{1}{3}\left(J_{\bar{E}}^{(3)}\,\eta''(x) + J_{\bar{E}}^{(4)}\,\xi'(x) - \frac{1}{2}\,J_{\bar{E}}^{(5)}\,\theta''''(x) + J_{\bar{E}}^{(6)}\,\delta'''(x)\right) - q_\psi(x) = 0, \tag{37e}$$

The elastostatic formulation written above consists of a system of five coupled differential equations governing the mechanical response of the proposed beam model.

Comprehensively, the system shows a strong interplay between axial and flexural behaviours and highlights the non-trivial c0oupling introduced by the functionally graded nature of the material and the higher-order kinematic assumptions. The formulation goes significantly beyond classical Reddy beam theory, introducing additional generalised stress/strain terms and enriching the equilibrium/kinematic formulation with physically consistent higher-order effects.

The admissible boundary conditions are directly derived from Eq. (20) and correspond to a total of 2^8 possible combinations, reflecting the binary choice between Dirichlet and Neumann boundary conditions for each of the eight generalised kinematic parameters.

6. Finite element formulation

The finite element method (FEM) is employed to discretise the governing differential equations (37) derived in the previous sections by approximating the generalised displacement fields through suitable shape functions.

The beam is discretised using one-dimensional finite elements having two end nodes. Each element interpolates the generalised displacement variables over its domain using appropriate shape functions, chosen on the basis of the highest order of spatial derivatives involved in the strain–displacement relations and the equilibrium equations, as well as based on the regularity requirements imposed by the weak form of the governing equations.

The variational framework ensures that the finite element discretisation retains the physical and mathematical consistency of the continuous model, allowing the accurate representation of bending, shear deformation and thickness stretch. The global stiffness matrix is assembled from the element matrices by standard FEM procedures and the resulting discrete system is solved under appropriate boundary conditions and external loading.

6.1. Weak form

The first step in developing the finite element model consists in formulating the weak form of the elastic equilibrium Eqs. (37), based on the principle of virtual displacements. The weak form is derived by multiplying each equilibrium equation by a corresponding virtual displacement, i.e. test function, and integrating over the finite element domain $\Sigma_e = \Omega \times [x_1, x_2]$, with $[x_1, x_2] \subseteq \left[-\frac{L}{2}, \frac{L}{2}\right]$, where x_1 and x_2 denote the axial coordinates of the two end nodes of the element along the beam axis.

Setting $\mathbf{d}(x)$ the vector collecting the generalised displacement fields

$$[\mathbf{d}(x)] = [w(x), v(x), \phi(x), \theta(x), \psi(x)]^T, \tag{38}$$

the generalised strain vector $\boldsymbol{\varepsilon}_\Omega(x)$ can be related to the previous vector in the following way

$$\boldsymbol{\varepsilon}_\Omega(x) = \boldsymbol{\Phi}(x)\,\mathbf{d}(x), \tag{39}$$

where $\boldsymbol{\Phi}(x)$ is the differential operator whose matrix representation reads

$$[\boldsymbol{\Phi}(x)] = \begin{bmatrix} \partial_x & 0 & 0 & 0 & 0 \\ 0 & 0 & \partial_x & 0 & 0 \\ 0 & 0 & 0 & \dfrac{\partial_x^2}{2} & 0 \\ 0 & -\alpha\,\partial_x^2 & \alpha\,\partial_x & 0 & -\dfrac{\partial_x^2}{3} \\ 0 & 0 & 0 & 1 & 0 \\ 0 & 0 & 0 & 0 & 2 \\ 0 & -\partial_x & 1 & 0 & 0 \\ 0 & -\beta\,\partial_x & \beta & 0 & 0 \end{bmatrix}. \tag{40}$$

Accordingly, the virtual work of internal forces over a finite element is given by

$$\delta W_I = \int_{x_1}^{x_2} \mathbf{K}_\Omega(x)\,\boldsymbol{\varepsilon}_\Omega(x) \cdot \boldsymbol{\Phi}(x)\,\delta\mathbf{d}(x)\,\mathrm{d}x, \tag{41}$$

where $\delta\mathbf{d}(x)$ is the variation of the displacement field.

Let us now set $\mathbf{q}^e(x)$ the vector collecting the distributed external loads acting along the element axis

$$[\mathbf{q}^e(x)] = \left[q_w(x),\ q_v(x),\ q_\phi(x),\ q_\theta(x),\ q_\psi(x)\right]^T, \tag{42}$$

and let $\mathbf{f}_i^e$ and $\mathbf{d}_i^e$ be the nodal vectors of generalised forces and displacements at the two element ends

$$\mathbf{f}_i^e = \left[\mathscr{F}_{w_i},\ \mathscr{F}_{v_i},\ \mathscr{F}_{\phi_i},\ \mathscr{F}_{\theta_i},\ \mathscr{F}_{\psi_i},\ \mathscr{F}_{v_i'},\ \mathscr{F}_{\theta_i'},\ \mathscr{F}_{\psi_i'}\right]^T, \quad \mathbf{d}_i^e = \left[w_i,\ v_i,\ \phi_i,\ \theta_i,\ \psi_i,\ v_i',\ \theta_i',\ \psi_i'\right]^T, \tag{43}$$

where $i = \{1, 2\}$ denotes the two nodes of a generic finite element. Hence, collecting the nodal vectors into global element vectors

$$\mathbf{f}^e = \begin{bmatrix}\mathbf{f}_1^e \\ \mathbf{f}_2^e\end{bmatrix}, \qquad \mathbf{d}^e = \begin{bmatrix}\mathbf{d}_1^e \\ \mathbf{d}_2^e\end{bmatrix}, \tag{44}$$

the virtual work of the external forces is given by

$$\delta W_E = \mathbf{f}^e \cdot \delta\mathbf{d}^e + \int_{x_1}^{x_2} \mathbf{q}^e(x) \cdot \delta\mathbf{d}(x)\,\mathrm{d}x. \tag{45}$$

According to previous results, invoking the principle of virtual displacements, the weak form of the elastic equilibrium problem reads

$$\int_{x_1}^{x_2} \mathbf{K}_\Omega(x)\,\boldsymbol{\varepsilon}_\Omega(x) \cdot \boldsymbol{\Phi}(x)\,\delta\mathbf{d}(x)\,\mathrm{d}x = \mathbf{f}^e \cdot \delta\mathbf{d}^e + \int_{x_1}^{x_2} \mathbf{q}^e(x) \cdot \delta\mathbf{d}(x)\,\mathrm{d}x. \tag{46}$$

6.2. Shape functions

From the variational formulation, the primary unknowns include the generalised displacements and their derivatives. Specifically, functions such as $w(x)$ and $\phi(x)$, which appear up to the first order derivatives, see, e.g., Eq. (12), are approximated using linear Lagrangian shape functions. In contrast, the displacement fields $v(x)$, $\theta(x)$ and $\psi(x)$, which appear up to second-order derivatives in the strain field, can be described using standard Hermite cubic interpolation functions in order to ensure sufficient differentiability and satisfy the minimum continuity requirements of the weak form.

This choice is also consistent with general finite element theory: when the weak form involves second-order derivatives, as in the case of the Euler–Bernoulli beam theory, the interpolation must represent both the field variable and its derivative at the nodes. This leads to the adoption of cubic Hermite polynomials, which are capable of satisfying four degrees of freedom, two function values and two first derivatives at the element nodes. In contrast, linear Lagrangian shape functions are sufficient for those variables whose weak form involves only first-order derivatives.

The generalised displacement field is interpolated as follows

$$w(x) = N_1(x)\,w_1 + N_2(x)\,w_2, \tag{47a}$$

$$v(x) = N_3(x)\,v_1 + N_5(x)\,v_1' + N_4(x)\,v_2 + N_6(x)\,v_2', \tag{47b}$$

$$\phi(x) = N_1(x)\,\phi_1 + N_2(x)\,\phi_2, \tag{47c}$$

$$\theta(x) = N_3(x)\,\theta_1 + N_5(x)\,\theta_1' + N_4(x)\,\theta_2 + N_6(x)\,\theta_2', \tag{47d}$$

$$\psi(x) = N_3(x)\,\psi_1 + N_5(x)\,\psi_1' + N_4(x)\,\psi_2 + N_6(x)\,\psi_2', \tag{47e}$$

where the shape functions $N_1, \ldots, N_6$ are defined as

$$\begin{aligned} N_1(x) &= \frac{1}{2} - \frac{x}{\ell}, & N_2(x) &= \frac{1}{2} + \frac{x}{\ell}, \\ N_3(x) &= 2\,\frac{x^3}{\ell^3} - \frac{3}{2}\,\frac{x}{\ell} + \frac{1}{2}, & N_4(x) &= -2\,\frac{x^3}{\ell^3} + \frac{3}{2}\,\frac{x}{\ell} + \frac{1}{2}, \\ N_5(x) &= \frac{x^3}{\ell^2} - \frac{1}{2}\,\frac{x^2}{\ell} - \frac{1}{4}\,x + \frac{\ell}{8}, & N_6(x) &= \frac{x^3}{\ell^2} + \frac{1}{2}\,\frac{x^2}{\ell} - \frac{1}{4}\,x - \frac{\ell}{8}, \end{aligned} \tag{48}$$

where ℓ denotes the finite element length.

Hence, the system of Eqs. (47) can be compactly expressed in matrix form as

$$\mathbf{d}(x) = \mathbf{N}(x)\,\mathbf{d}^e, \tag{49}$$

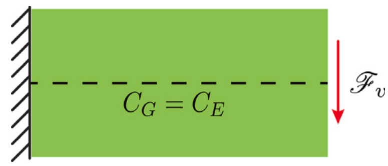

Fig. 2. Geometry and boundary conditions of the transversally loaded homogeneous cantilever beam. The beam, with a uniform Young modulus distribution, is clamped at the left end and subjected to a downward concentrated transverse force $\mathscr{F}_v$ applied at the free end. The dashed line indicates the axis of the beam coincident with the locus of the geometric centroids of the beam cross sections.

where $\mathbf{d}(x)$ is defined in Eq. (38), $\mathbf{d}^e$ in Eq. (44) and $\mathbf{N}(x)$ is the displacement operator. The matrix representation of the previous equation is

$$
\begin{bmatrix} w(x) \\ v(x) \\ \phi(x) \\ \theta(x) \\ \psi(x) \end{bmatrix} = \begin{bmatrix}
N_1 & 0 & 0 & 0 & 0 & 0 & 0 & 0 & N_2 & 0 & 0 & 0 & 0 & 0 & 0 & 0 \\
0 & N_3 & 0 & 0 & 0 & N_5 & 0 & 0 & 0 & N_4 & 0 & 0 & 0 & N_6 & 0 & 0 \\
0 & 0 & N_1 & 0 & 0 & 0 & 0 & 0 & 0 & 0 & N_2 & 0 & 0 & 0 & 0 & 0 \\
0 & 0 & 0 & N_3 & 0 & 0 & N_5 & 0 & 0 & 0 & 0 & N_4 & 0 & 0 & N_6 & 0 \\
0 & 0 & 0 & 0 & N_3 & 0 & 0 & N_5 & 0 & 0 & 0 & 0 & N_4 & 0 & 0 & N_6
\end{bmatrix} \mathbf{d}^e \tag{50}
$$

with $[\mathbf{d}^e]^T = \begin{bmatrix} w_1 & v_1 & \phi_1 & \theta_1 & \psi_1 & v_1' & \theta_1' & \psi_1' & w_2 & v_2 & \phi_2 & \theta_2 & \psi_2 & v_2' & \theta_2' & \psi_2' \end{bmatrix}$. Notice that the explicit dependence of the shape functions $N_1, \ldots, N_6$ on the local abscissa x is omitted for brevity.

According to Eq. (49), formula (39) specialises to

$$
\boldsymbol{\varepsilon}_\Omega(x) = \boldsymbol{\Phi}(x)\,\mathbf{N}(x)\,\mathbf{d}^e = \mathbf{B}(x)\,\mathbf{d}^e \tag{51}
$$

being $\mathbf{B}(x)$ the strain operator whose matrix representation is

$$
[\mathbf{B}(x)] = \begin{bmatrix}
N_1' & 0 & 0 & 0 & 0 & 0 & 0 & 0 & N_2' & 0 & 0 & 0 & 0 & 0 & 0 & 0 \\
0 & 0 & N_1' & 0 & 0 & 0 & 0 & 0 & 0 & 0 & N_2' & 0 & 0 & 0 & 0 & 0 \\
0 & 0 & 0 & \frac{N_3''}{2} & 0 & 0 & \frac{N_5''}{2} & 0 & 0 & 0 & 0 & \frac{N_4''}{2} & 0 & 0 & \frac{N_6''}{2} & 0 \\
0 & -\alpha\,N_3'' & \alpha\,N_1' & 0 & -\frac{N_3''}{3} & -\alpha\,N_5'' & 0 & -\frac{N_5''}{3} & 0 & -\alpha\,N_4'' & \alpha\,N_2' & 0 & -\frac{N_4''}{3} & -\alpha\,N_6'' & 0 & -\frac{N_6''}{3} \\
0 & 0 & 0 & N_3 & 0 & 0 & N_5 & 0 & 0 & 0 & 0 & N_4 & 0 & 0 & N_6 & 0 \\
0 & 0 & 0 & 0 & 2\,N_3 & 0 & 0 & 2\,N_5 & 0 & 0 & 0 & 0 & 2\,N_4 & 0 & 0 & 2\,N_6 \\
0 & -N_3' & N_1 & 0 & 0 & -N_5' & 0 & 0 & 0 & -N_4' & N_2 & 0 & 0 & -N_6' & 0 & 0 \\
0 & -\beta\,N_3' & \beta\,N_1 & 0 & 0 & -\beta\,N_5' & 0 & 0 & 0 & -\beta\,N_4' & \beta\,N_2 & 0 & 0 & -\beta\,N_6' & 0 & 0
\end{bmatrix}. \tag{52}
$$

6.3. Derivation of the stiffness matrix and force vector

The substitution of Eqs. (49) and (51) into the weak form (46) yields

$$
\int_{x_1}^{x_2} \mathbf{B}^T(x)\,\mathbf{K}_\Omega(x)\,\mathbf{B}(x)\,\mathrm{d}x\,\mathbf{d}^e \cdot \delta\mathbf{d}^e = \mathbf{f}^e \cdot \delta\mathbf{d}^e + \int_{x_1}^{x_2} \mathbf{N}^T(x)\,\mathbf{q}^e(x)\,\mathrm{d}x \cdot \delta\mathbf{d}^e, \tag{53}
$$

where, for the arbitrariness of $\delta\mathbf{d}^e$, we get

$$
\int_{x_1}^{x_2} \mathbf{B}^T(x)\,\mathbf{K}_\Omega(x)\,\mathbf{B}(x)\,\mathrm{d}x\,\mathbf{d}^e = \mathbf{f}^e + \int_{x_1}^{x_2} \mathbf{N}^T(x)\,\mathbf{q}^e(x)\,\mathrm{d}x. \tag{54}
$$

Furthermore, from a mechanical point of view, the previous integrals on the left- and right-hand side are characteristic quantities associated with a beam element. Specifically

$$
\begin{aligned}
\mathbf{K}_{\Sigma_e} &= \int_{x_1}^{x_2} \mathbf{B}^T(x)\,\mathbf{K}_\Omega(x)\,\mathbf{B}(x)\,\mathrm{d}x, \\
\mathbf{f}_q^e &= \int_{x_1}^{x_2} \mathbf{N}^T(x)\,\mathbf{q}^e(x)\,\mathrm{d}x,
\end{aligned} \tag{55}
$$

where $\mathbf{K}_{\Sigma_e}$ is the element stiffness tensor and $\mathbf{f}_q^e$ is the element nodal force vector associated with distributed loads.

Accordingly, Eq. (54) specialises to the following algebraic form

$$
\mathbf{K}_{\Sigma_e}\,\mathbf{d}^e = \mathbf{f}^e + \mathbf{f}_q^e, \tag{56}
$$

which represents the finite element equilibrium equation for a generic element Σ_e. In order to derive the global finite element model, the algebraic relations of all elements are assembled. This assembly process is carried out by enforcing continuity of the generalised displacements and balance of the generalised stresses at the interface between elements.

Once the global system is assembled, the prescribed boundary conditions are applied. These must be expressed as known values of the duality pairs at the nodes, depending on whether displacements or forces are imposed. The resulting system of algebraic equations is then solved to obtain the unknown nodal values.

Finally, the solution at internal points of the domain, such as displacement, strain or stress fields, is obtained by interpolation of the nodal values of displacements and application of the constitutive and strain–displacement relations.

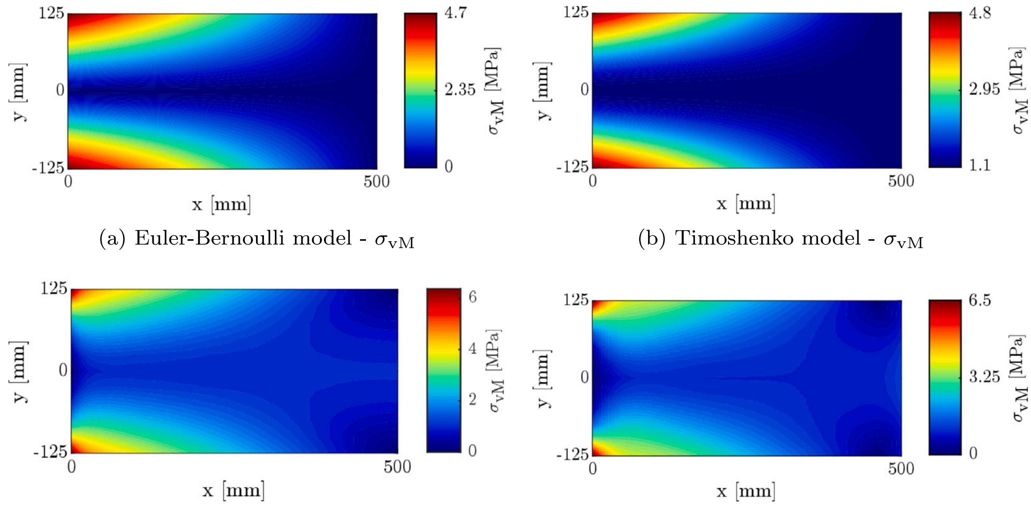

(a) Euler-Bernoulli model - σ_{vM} (b) Timoshenko model - σ_{vM} (c) Reddy model - σ_{vM} (d) Proposed model - σ_{vM}

Fig. 3. Comparison of the von Mises equivalent stress distributions σ_{vM} obtained from four beam models for a transversally loaded homogeneous cantilever beam. (a) Euler–Bernoulli model; (b) Timoshenko model; (c) Reddy model; (d) Proposed model.

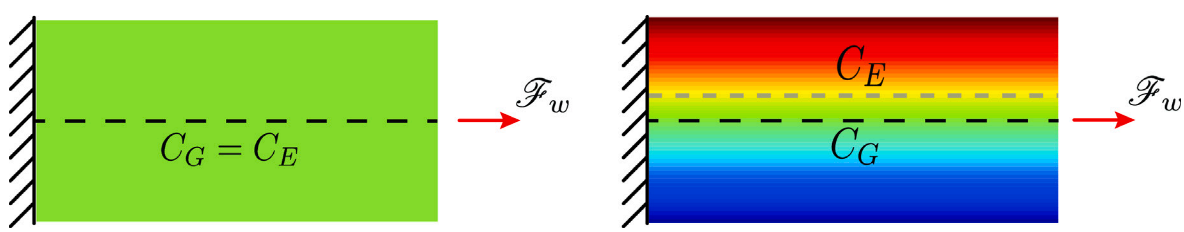

(a) Homogeneous Young modulus distribution (b) Linear Young modulus distribution

Fig. 4. Geometry and boundary conditions of the axially loaded cantilever beam. (a) Homogeneous beam with a uniform Young modulus distribution. (b) Functionally graded beam in which the Young modulus varies linearly along the beam thickness according to Eq. (57). The black dashed line denotes the locus of the geometric centroids C_G of the cross sections, whereas the green dashed line indicates the locus of the elastic centroids C_E. (For interpretation of the references to colour in this figure legend, the reader is referred to the web version of this article.)

7. Numerical results

The proposed beam formulation is assessed by a series of numerical investigations. The aim is to verify the accuracy and effectiveness of the model in predicting the structural response of functionally graded beams under different loading and boundary conditions.

All numerical results are validated with those obtained using an in-house FEM software for two-dimensional continua, employing four-node linear quadrilateral elements with Selective Reduced Integration (Zienkiewicz and Taylor, 2000a,b). Additionally, validation against benchmark solutions available in the literature is performed.

7.1. Transversally loaded cantilever beam

To highlight the capability of the proposed beam model in capturing enriched stress states, a preliminary comparison is carried out between the proposed Reddy-based beam model and the canonical beam theories by Euler–Bernoulli, Timoshenko and the classical Reddy beam. The example case consists of a homogeneous cantilever beam of length $L = 0.5\,\mathrm{m}$, thickness $h = 0.5\,L$ and width $b = 0.2L$, subjected to a downward concentrated transverse force $\mathscr{F}_v = 10\,\mathrm{kN}$ applied at the free end $x = L$, as schematically shown in Fig. 2. The Young modulus and the Poisson ratio are set 200 GPa and 0.3, respectively. The clamped end at $x = 0$ is obtained by setting the following boundary conditions: $w = v = \phi = \theta = \psi = v' = \theta' = \psi' = 0$.

Fig. 3 compares the von Mises equivalent stress σ_{vM} computed with the four beam models, i.e. Euler–Bernoulli beam model, Fig. 3(a); Timoshenko beam model, Fig. 3(b); the classical Reddy beam model, Fig. 3(c); the extended Reddy-based beam model, Fig. 3(d). Qualitatively, the Euler–Bernoulli and Timoshenko solutions produce smooth and bending-dominated stress fields, with the maximum σ_{vM} located at the clamped section and a linear variation along the beam thickness. The Timoshenko model predicts slightly higher stress levels due to the contribution of shear deformation. In contrast, both the classical Reddy model and the proposed model exhibit a von Mises stress field that displays localised peaks near the fixed boundary. While the classical Reddy model improves upon first-order theories by providing a non-linear axial stress and a quadratic shear stress distribution, it inherently fails to capture thickness stretch effects. The proposed model, thanks to the additional kinematic fields, accounts for the transverse normal stress and higher-order shear components.

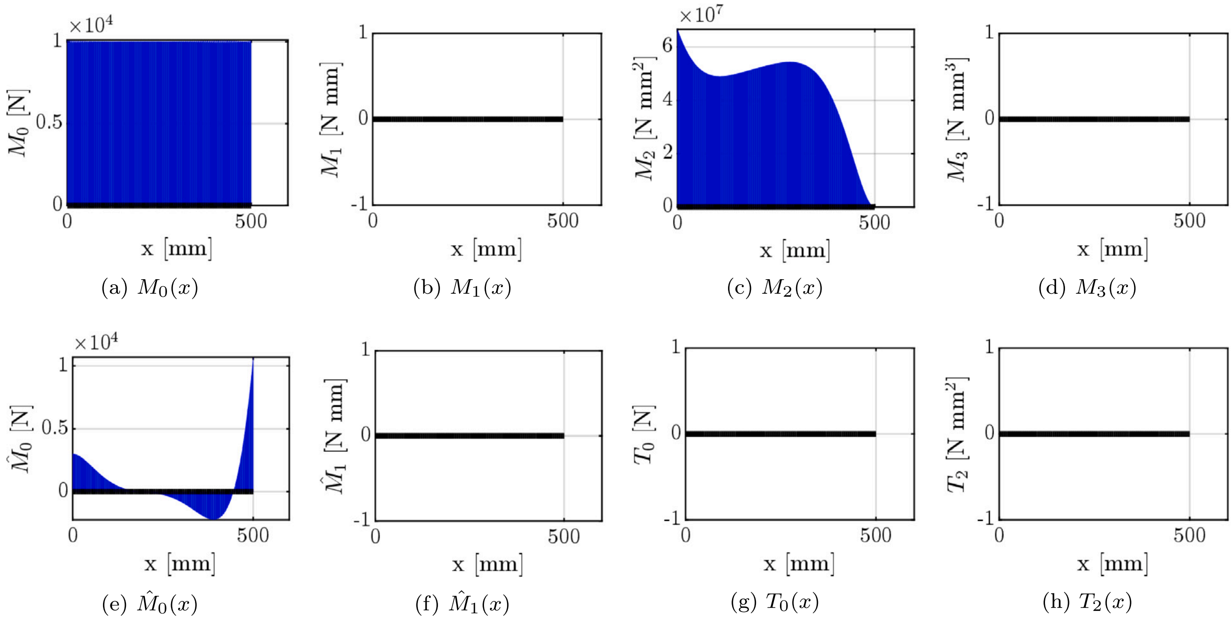

Fig. 5. Generalised stresses of the axially loaded homogeneous cantilever beam.

7.2. Axially loaded cantilever beam

We now consider a cantilever beam of length $L = 0.5\,\mathrm{m}$, thickness $h = 0.5L$ and width $b = 0.2L$, subjected to an axial tensile force $\mathscr{F}_w = 10\,\mathrm{kN}$ applied at the free end $x = L$.

We analyse two distinct cases in which the cantilever beam is assumed to be made of two materials having different Young modulus distributions: the first case, discussed in Section 7.2.1, corresponds to a homogeneous distribution and is assumed as a reference benchmark; the second case, shown in Section 7.2.2, considers a linear variation along the thickness of the cross section, thereby highlighting the ability of the formulation to handle graded materials. In both cases the Poisson ratio is set $\nu = 0.3$. The geometry and loading conditions of the two cases are illustrated in Fig. 4.

Furthermore, the numerical results of the proposed formulation are compared with those obtained from an in-house FE software of a 2D continuum. Additionally, restricted to the homogeneous case investigated in Section 7.2.1, a direct comparison with the classical Reddy beam theory is also provided. Both one-dimensional beam models (i.e., the classical Reddy and the proposed 1D continuum) are discretised into 100 finite elements, while the 2D model is meshed with a grid of 100×10 elements. In the 2D continuum FE model, the concentrated force is not prescribed at the free end as in the 1D beam models, but rather by prescribing the displacement components u_x and u_y at the 11 nodes distributed along the thickness of the free cross section. These nodal displacements are extracted from the results of the proposed 1D beam analysis, where the axial force was applied, thus ensuring a consistent and comparable loading condition among the models.

7.2.1. Homogeneous Young modulus distribution

We assume a constant Young modulus $E = 200$ GPa along the cross section thickness, providing a reference case for assessing the capability of the proposed model to reproduce consistent stress and displacement distributions under a concentrated axial force at the free end.

In Fig. 5 are illustrated the generalised stresses of the homogeneous beam. For this example, the axial force $M_0(x)$ is constant and its value is equal to the norm of applied force $\mathscr{F}_w$ at the free end while the bending moment $M_1(x)$ is constantly zero. In addition, non-zero values of $M_2(x)$ and $\hat{M}_0(x)$ are observed. The latter is directly related to the thickness stretch of the cross section induced by the axial tensile force at the free end.

For completeness, Fig. 6 reports the generalised displacements. In particular, the axial displacement at the free end, $w(x = L)$, shown in Fig. 6(a), exceeds the analytical value $\mathscr{F}_w\, L/(EA)$ provided by classical beam theories, such as Euler–Bernoulli. This difference can be ascribed to the relaxation of the kinematic constraint that, in traditional models, prevents the cross section from undergoing transverse contraction or expansion.

The stress and displacement fields obtained with the classical Reddy beam model, the proposed beam model (both 1D continuum) and the two-dimensional continuum (2D continuum) are compared in the left, middle and right columns, respectively, of Figs. 7 and 8. Both stress and displacement distributions exhibit symmetry with respect to the mid-plane of the cross section. The classical Reddy beam model predicts a uniform axial stress σ_x and an axial displacement u_x that is constant across the thickness. Furthermore, the transverse displacement u_y and transverse normal stress σ_y are identically zero. In contrast, the proposed model shows not only a non-uniform axial stress component σ_x but also the transverse normal stress σ_y due to the transverse contraction of the cross section. It is worth noting that the transverse stress σ_y is of the same order of magnitude as the axial stress σ_x, highlighting the coupling effect introduced by the Poisson effect. Furthermore, localised effects can be observed where boundary conditions are applied, both in stress and displacement fields. Thus, such a model leads to a richer stress state showing how the stress components σ_x and σ_y are locally influenced by the external forces.

The comparison with the 2D FE model confirms that the proposed beam model is able to capture displacement fields along the element axis as well as stress fields of the same order of magnitude as those obtained with the 2D formulation. However, a variation emerges in terms of the shear stress field τ_{xy}, see, e.g., Fig. 7(h) and (i). In both the classical Reddy and the proposed 1D models, τ_{xy} is identically zero, whereas the 2D analysis reveals localised shear stress distributions near the end sections. This stress field displayed in the 2D model is induced by the contraction

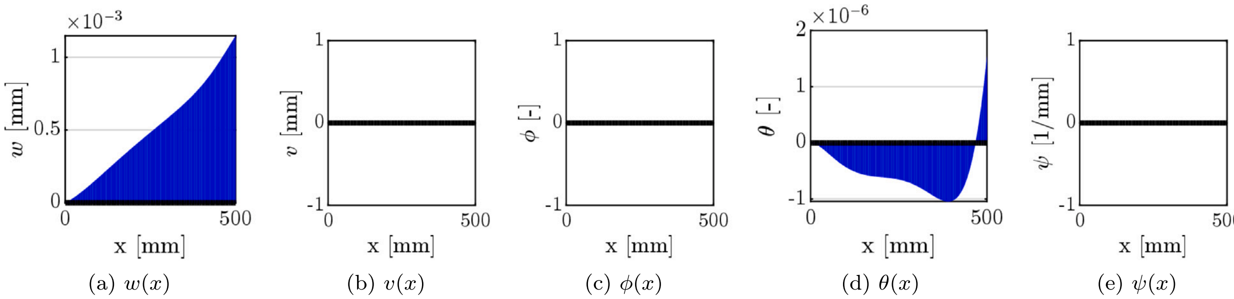

Fig. 6. Generalised displacements of the axially loaded homogeneous cantilever beam.

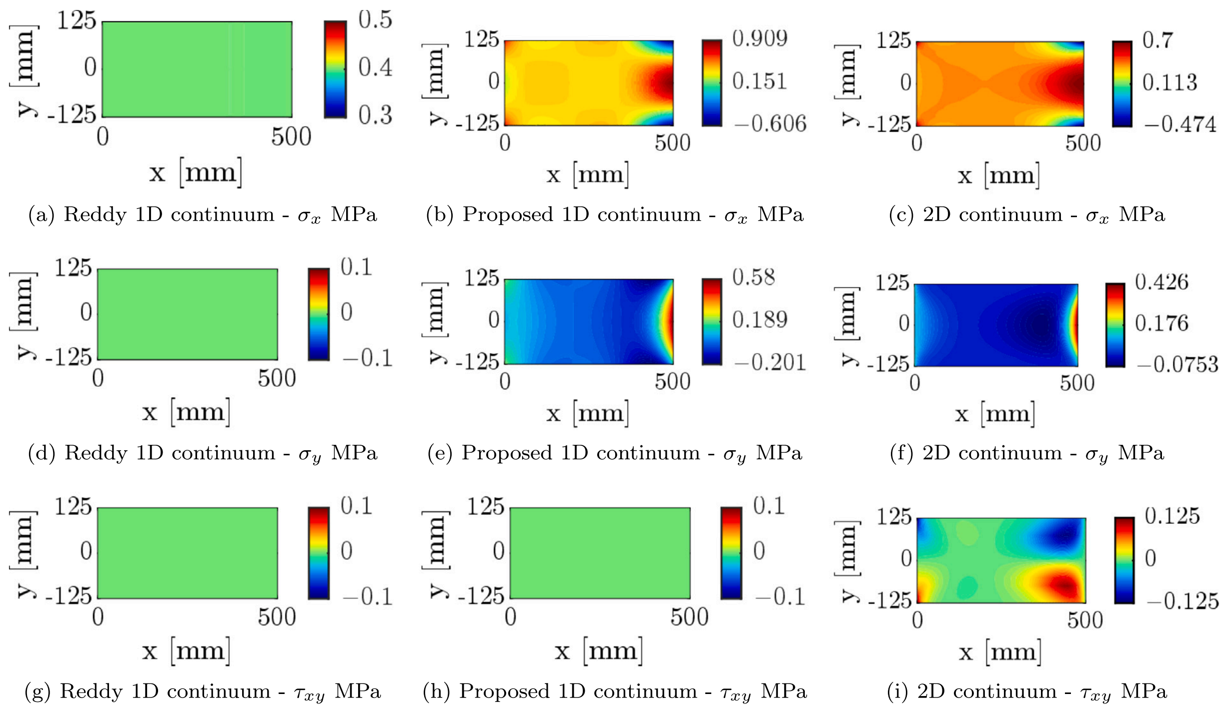

Fig. 7. Stress fields of the axially loaded homogeneous cantilever beam. Left column: classical Reddy one-dimensional beam model; middle column: proposed one-dimensional beam model; right column: two-dimensional continuum model.

of the cross sections. The proposed 1D model is not able to display this additional stress field because of its kinematic formulation. Indeed, as shown in Section 3, the shear strain is the same as that obtained with the classical Reddy beam model, see Eqs. $(6)_2$ and $(12)_3$. Hence, to properly account for shear stress and strain due to lateral contraction or expansion of the cross section, a further enrichment of the kinematics would be required. Nevertheless, when focusing on sections sufficiently far from the boundaries, where the stress state is not influenced by the specific applied force/displacement field, the results of the two models are in good agreement.

7.2.2. Linear Young modulus distribution

In the second example, the cantilever beam is assumed to be made of a functionally graded material characterised by a linear variation of the Young modulus along the thickness of the cross section following the expression

$$E(y) = \frac{E_b + E_t}{2} + \frac{E_t - E_b}{h}\, y, \tag{57}$$

where $E_b = 50$ GPa and $E_t = 300$ GPa are the values of the Young modulus at the bottom and top of cross section, respectively. Fig. 9(a) illustrates the geometry of the cross sections with the spatial variation of the Young modulus. In the same figure, both the geometric centroid C_G and the elastic centroid C_E are shown. The elastic centroid C_E is evaluated as $J_E^{(1)}/J_E^{(0)}$, making use of formula (33). As expected, the position of C_E is shifted towards the stiffer portion of the section, i.e., in the direction of increasing $E(y)$.

In contrast to the homogeneous case, Fig. 10, in which the generalised displacement fields are plotted, shows non-vanishing values of $v(x)$, $\phi(x)$ and $\psi(x)$. This behaviour is directly related to the misalignment between the elastic and geometric centroids: when these two points do not coincide, an axial force not only induces axial deformation but also generates bending of the beam.

Hence, the stress and displacement field do not exhibit symmetry with respect to the mid-plane, as shown in Figs. 11 and 12. The agreement with the 2D FE results confirms that the model accurately describes both the bending behaviour and the stress field associated with the material gradation. A good qualitative agreement can be observed for the axial stress σ_x and transverse stress σ_y, both in terms of the distribution along

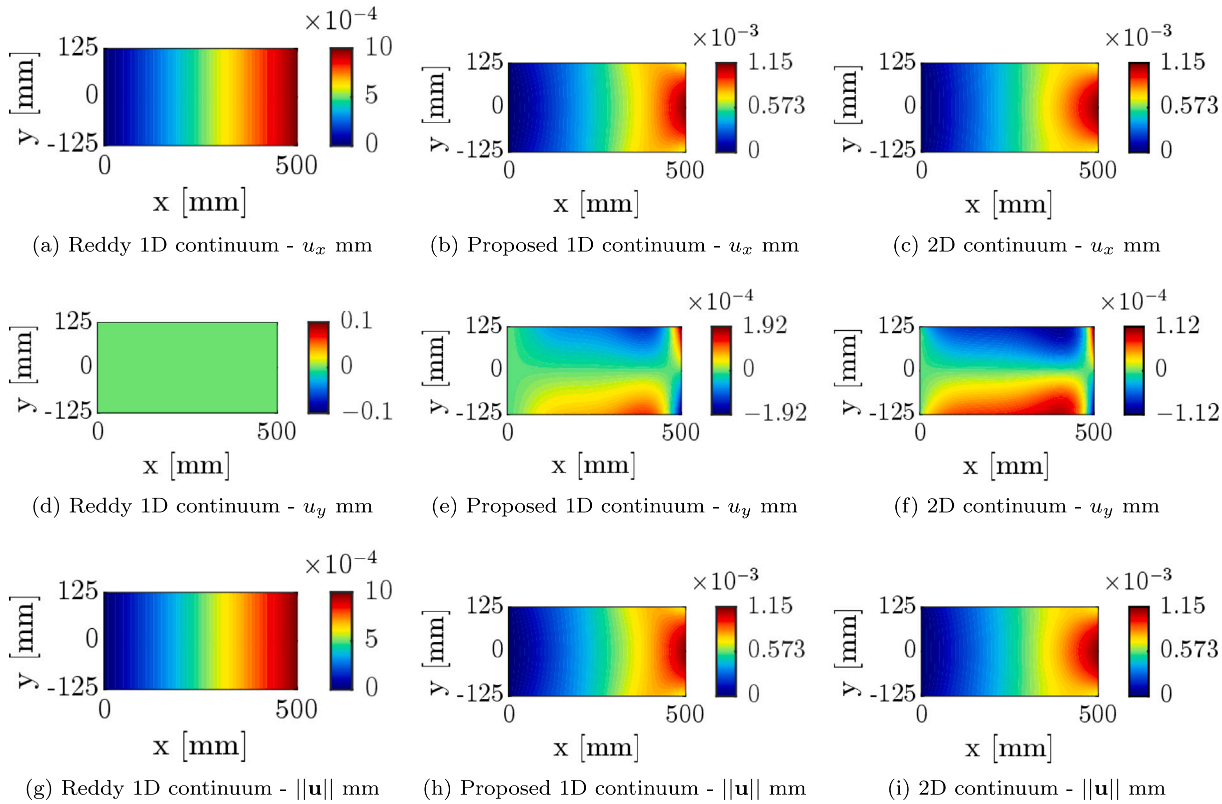

(a) Reddy 1D continuum - u_x mm (b) Proposed 1D continuum - u_x mm (c) 2D continuum - u_x mm

(d) Reddy 1D continuum - u_y mm (e) Proposed 1D continuum - u_y mm (f) 2D continuum - u_y mm

(g) Reddy 1D continuum - $||\mathbf{u}||$ mm (h) Proposed 1D continuum - $||\mathbf{u}||$ mm (i) 2D continuum - $||\mathbf{u}||$ mm

Fig. 8. Displacement fields of the axially loaded homogeneous cantilever beam. Left column: classical Reddy one-dimensional beam model; middle column: proposed one-dimensional beam model; right column: two-dimensional continuum model.

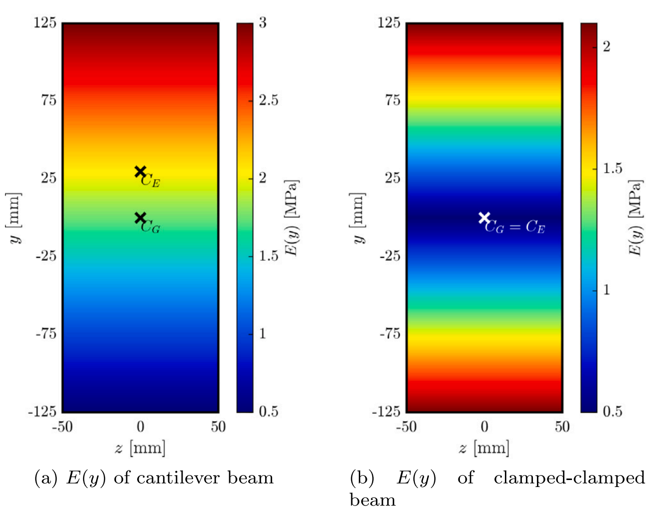

(a) $E(y)$ of cantilever beam (b) $E(y)$ of clamped-clamped beam

Fig. 9. Distributions of the Young modulus along the cross section of the FG cantilever (a) and clamped-clamped (b) beams. In (a), the material gradation follows the linear law specified in Eq. (57), whereas in (b) the Young modulus varies quadratically through the thickness according to Eq. (58).

the beam axis and the order of magnitude of the values, see Fig. 11(a)–(d). The shear stresses τ_{xy} exhibit more pronounced differences, especially near the constrained and loaded ends, see Fig. 11(e)–(f). Nonetheless, the beam formulation is able to recover the overall stress trends far from boundary conditions.

7.3. Transversally loaded clamped-clamped beam

We consider a clamped–clamped beam having the same length and rectangular cross section introduced in the previous subsection. The material is functionally graded along the thickness and is characterised by a quadratic variation of the Young modulus, prescribed as

$$E(y) = E_0 + (E_{tb} - E_0)\,\frac{4}{h^2}\,y^2, \tag{58}$$

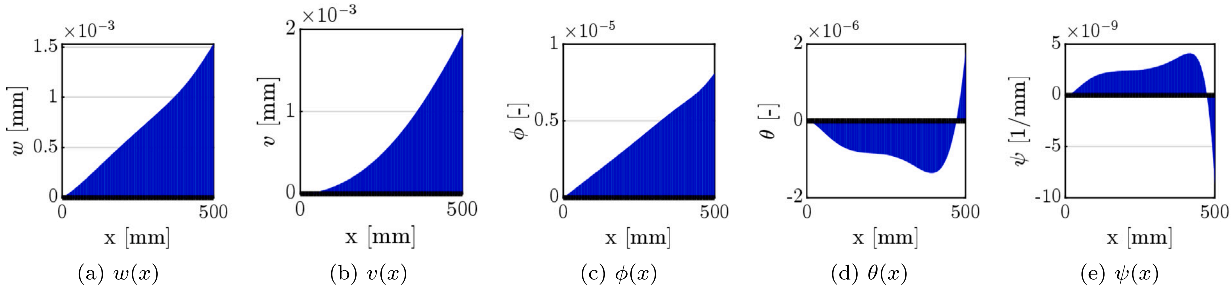

Fig. 10. Generalised displacements of the FG cantilever beam.

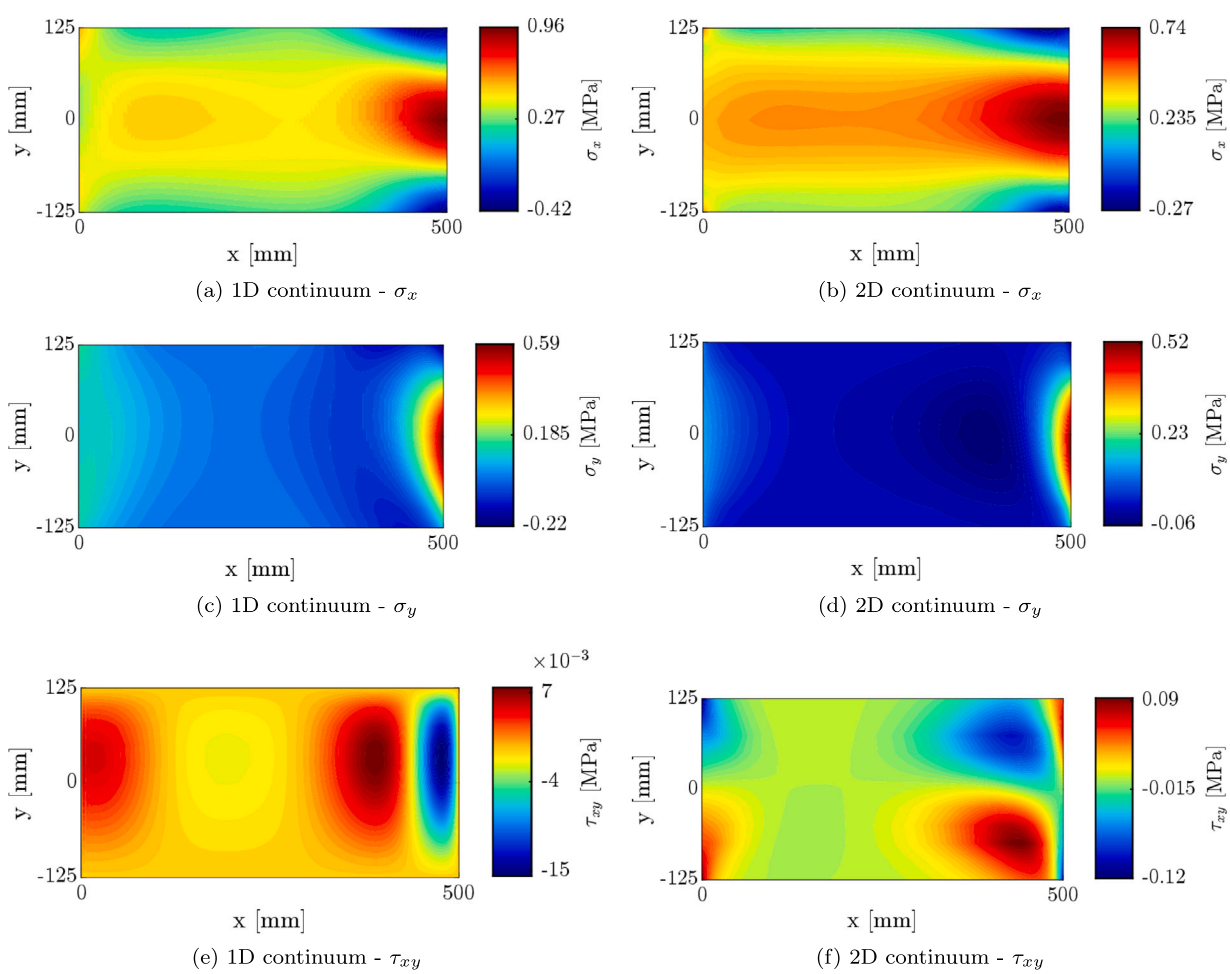

Fig. 11. Stress fields of the axially loaded FG cantilever beam with a linear variation of the Young modulus along the thickness specified in Eq. (57). Left column: proposed one-dimensional beam formulation; right column: two-dimensional finite element continuum model.

where y is the transverse coordinate measured from the geometric centroid, $E_0 = 50$ GPa and $E_{tb} = 210$ GPa are the Young moduli at $y = 0$ and $y = \pm h/2$ of cross section, respectively, see, e.g., Fig. 9(b). The elastic centroid C_E coincides with the geometric one C_G due to the symmetric distribution of the Young modulus about the midplane of the cross section, see Fig. 9(b). Additionally, the Poisson ratio is still set $\nu = 0.3$.

The mechanical response of the beam is investigated under two distinct transverse loading configurations, schematically illustrated in Fig. 13. In the first case, shown in Fig. 13(a), the beam is subjected at midspan $x = L/2$ to a pair of opposite concentrated forces $\mathscr{F}_\theta$. In the second loading condition, depicted in Fig. 13(b), the beam is loaded by a distributed higher-order forces of intensity q_ψ acting along the entire span. It should be noted that the latter illustration is purely schematic, as the physical interpretation of higher-order distributed forces is not straightforward and primarily serves to represent the generalised loading conditions accounted for in the proposed formulation.

The numerical analyses for both loading configurations are validated by comparison with the analysis of the two-dimensional continuum. The discretisation adopted for the 1D and 2D models is identical to that employed in the cantilever beam. The boundary conditions of the 2D model are prescribed in kinematic form by imposing at the nodes of the loaded cross sections the displacement field obtained from the 1D beam solution, thereby ensuring a consistent and meaningful comparison between the two formulations.

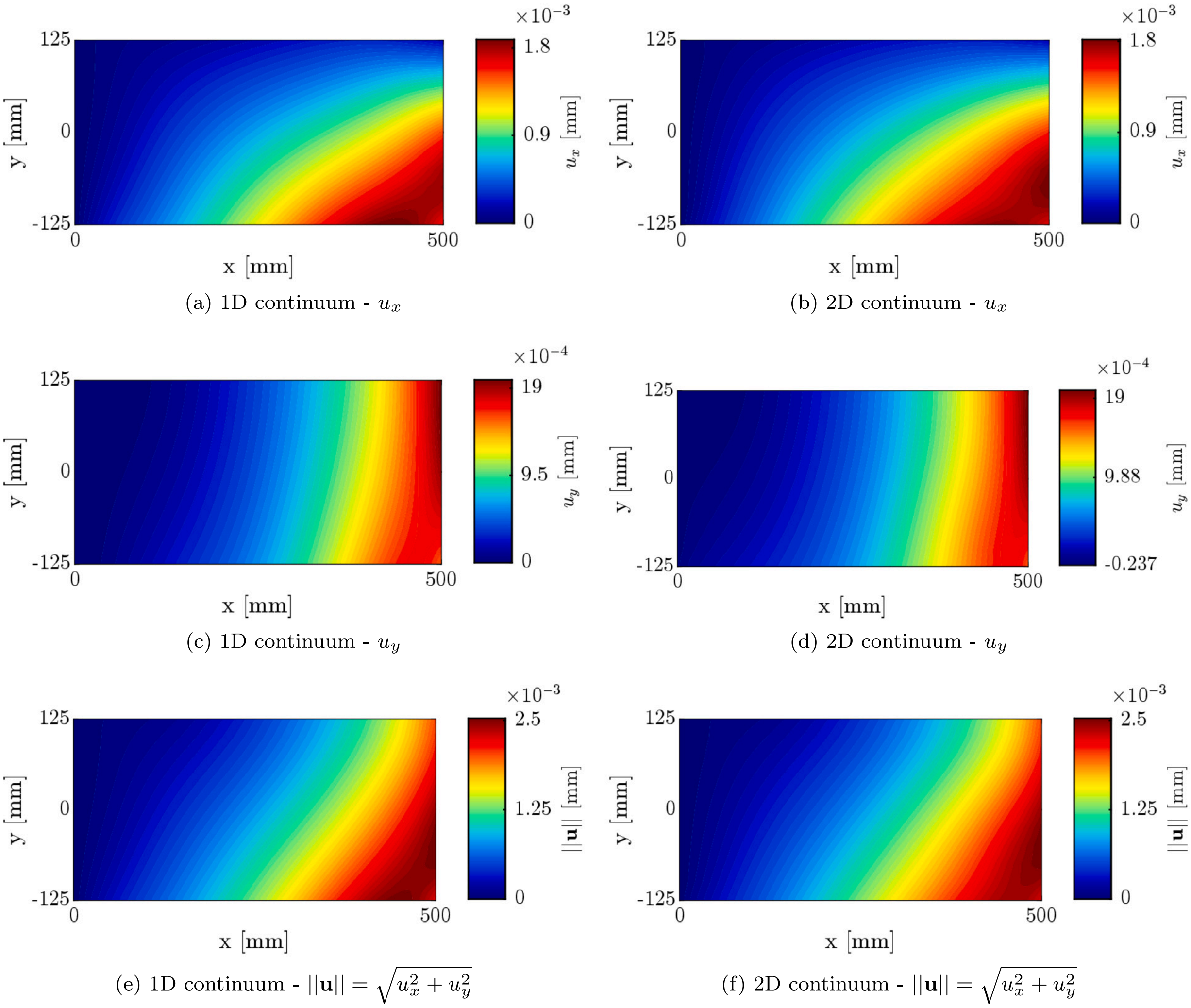

(a) 1D continuum - u_x (b) 2D continuum - u_x

(c) 1D continuum - u_y (d) 2D continuum - u_y

(e) 1D continuum - $||\mathbf{u}|| = \sqrt{u_x^2 + u_y^2}$ (f) 2D continuum - $||\mathbf{u}|| = \sqrt{u_x^2 + u_y^2}$

Fig. 12. Displacement fields of the axially loaded FG cantilever beam with a linear variation of the Young modulus along the thickness specified in Eq. (57). Left column: proposed one-dimensional beam formulation; right column: two-dimensional finite element continuum model.

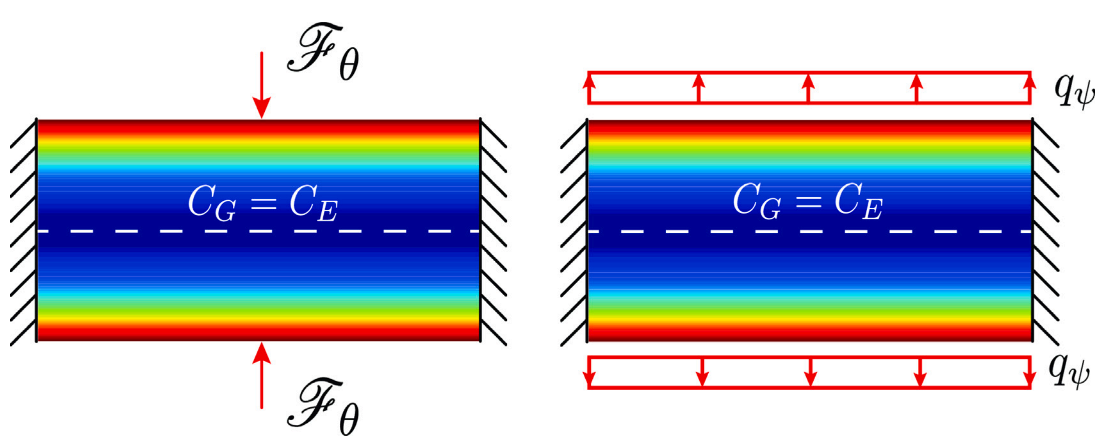

(a) Pair of concentrated forces applied at midspan (b) Distributed load of high-order forces

Fig. 13. Geometry and boundary conditions of the transversally loaded FG clamped–clamped beam. (a) Application of a pair of concentrated forces $\mathscr{F}_\theta$ at midspan, energetically dual to the generalised displacement $\theta(x = L/2)$. (b) Application of a uniformly distributed load q_ψ, energetically dual to the generalised displacement $\psi(x)$.

7.3.1. Concentrated forces

The first loading condition consists of a pair of concentrated forces applied at midspan $\mathscr{F}_\theta = -10$ kN mm, as illustrated in Fig. 13(a). This loading condition is peculiar to the proposed beam formulation and has no counterpart in the canonical beam theories such as the ones due to Euler–Bernoulli, Timoshenko or Reddy, which do not include higher-order generalised forces associated with the additional kinematic fields introduced herein. Specifically, the concentrated forces $\mathscr{F}_\theta$ is energetically dual to the generalised displacement component $\theta(x)$, which governs the linear contraction or expansion of the cross section, as defined in Eq. (7).

The stress distributions obtained from the proposed one-dimensional formulation (left column) and from the two-dimensional continuum model (right column) are compared in Fig. 14. Overall, despite the simplified formulation, the present beam model satisfactorily reproduces the magnitudes of the stress components predicted by the 2D reference solution.

In particular, the longitudinal normal stress σ_x (Fig. 14(a)–(b)) exhibits a symmetric pattern with respect to the beam midspan and comparable stress levels, although the 1D model slightly underestimates the local peak values near the load application points, where the 2D continuum shows a more localised stress field. The transverse normal stress σ_y (Fig. 14(c)–(d)) is captured in terms of order of magnitude, but the 2D model displays a more pronounced variation across the thickness . Finally, the shear stress τ_{xy} (Fig. 14(e)–(f)) is identically zero in the proposed 1D formulation, consistently with the assumed uncoupling between normal and tangential strain components, whereas the 2D continuum solution reveals localised shear stress concentrations at the point of load application.

The comparison between the displacement fields obtained from the 1D and 2D formulations, reported in Fig. 15, confirms the overall consistency between the two models. The localised effect induced by the concentrated loading condition exhibits a different spatial decay in the two models. In the proposed 1D formulation, the effect associated with $\mathscr{F}_\theta$ extends over a larger portion of the span before vanishing, whereas in the 2D continuum model the same effect is confined to a narrower region around the load application point.

Despite these differences, the amplitude and qualitative shape of the stress and displacement fields remain in very good agreement, demonstrating that the proposed model captures the mechanical features of this unconventional loading case while preserving a physically consistent response along the beam.

In summary, the comparison highlights the capability of the proposed beam formulation to accurately reproduce the global stress and displacement distributions and overall structural response.

7.3.2. Distributed load

The second loading condition consists of a pair of distributed loads $q_\psi = -10\,000$ kN mm^2 applied along the beam span, as illustrated in Fig. 13(b). This load is energetically dual to the generalised displacement component $\psi(x)$, which manages the quadratic part of the contraction or expansion of the cross section, as defined in Eq. (7).

The corresponding stress and displacement fields obtained from the 1D and 2D formulations are reported in Figs. 16 and 17, respectively.

The comparison shows that the overall shape and distribution of both stress and displacement fields are well captured by the proposed 1D beam model, which reproduces the mechanical response observed in the 2D continuum. Minor quantitative differences are observed in the stress magnitude, with the 1D model slightly overestimating the stress levels. This discrepancy is mainly attributed to the simplified kinematic assumptions of the beam formulation, which, while showing higher-order effects introduced by the generalised fields, cannot fully reproduce the local stress gradients present in the 2D reference solution.

7.4. Comparison of maximum transverse displacements for FG beams

To assess the accuracy and validate the proposed FG beam model, the current results are compared with those reported in the literature by Li et al. (2019), Ruocco and Reddy (2023b) and Müsevitoğlu et al. (2025). The reference data correspond to classical Reddy-type higher-order shear deformation theories applied to FG beams.

The comparison is carried out in terms of the maximum absolute transverse displacements for three boundary conditions, namely cantilever (CF), clamped–clamped (CC) and simply supported (SS) beams. The loading conditions and span lengths are illustrated in Fig. 18. All beams feature a rectangular cross section having width $b = 50$ mm and thickness $h = 200$ mm.

The material is assumed to be functionally graded along the thickness direction according to the Voigt's rule of mixtures. Hence, the Young modulus is expressed as (Wakashima et al., 1990)

$$E(y) = (E_t - E_b)\left(\frac{y}{h} + \frac{1}{2}\right)^m + E_b, \tag{59}$$

where $E_t = 380$ GPa and $E_b = 70$ GPa are the Young moduli at the top and bottom surfaces of the beam, respectively, h is the total thickness, y is the coordinate measured from the cross section geometric centroid and m is the power-law exponent controlling the material gradation. Specifically, for $m = 0$, the beam behaves as a homogeneous material with $E(y) = E_t$. When $m = 1$, Young modulus varies linearly from E_b at the bottom surface to E_t at the top surface. For larger values of m, the increase of $E(y)$ from E_b to E_t becomes steeper, producing a stiffer region concentrated near the top surface and a nearly constant modulus close to E_b elsewhere. In the limiting case $m \to \infty$, the Young modulus tends to E_b throughout almost the entire thickness. Poisson ratio is assumed to be constant and equal to $\nu = 0.3$.

Table 1 lists the maximum absolute transverse displacements $|v_{\max}|$ in millimetres for the three boundary conditions and several values of the power-law exponent m. The results obtained from the proposed model are compared with those reported in the literature by Li et al. (2019), Ruocco and Reddy (2023a,b) and Müsevitoğlu et al. (2025).

For $m = 0$, corresponding to a homogeneous beam, all models provide nearly identical displacements, confirming the correctness of the proposed implementation. As the power-law index m increases, the three beams become more compliant, leading to progressively larger transverse displacements.

Overall, a very good agreement is observed between the present results and the reference solutions available in the literature. The small differences found for all the analysed values of the power-law index m are mainly due to the different structural models being compared, namely the classical Reddy beam theory adopted in the reference studies and the present extended formulation accounting for the thickness stretch. In addition, for the specific cases $m = 0.2$ and $m = 0.5$, a further source of discrepancy arises from the numerical approximation adopted to evaluate

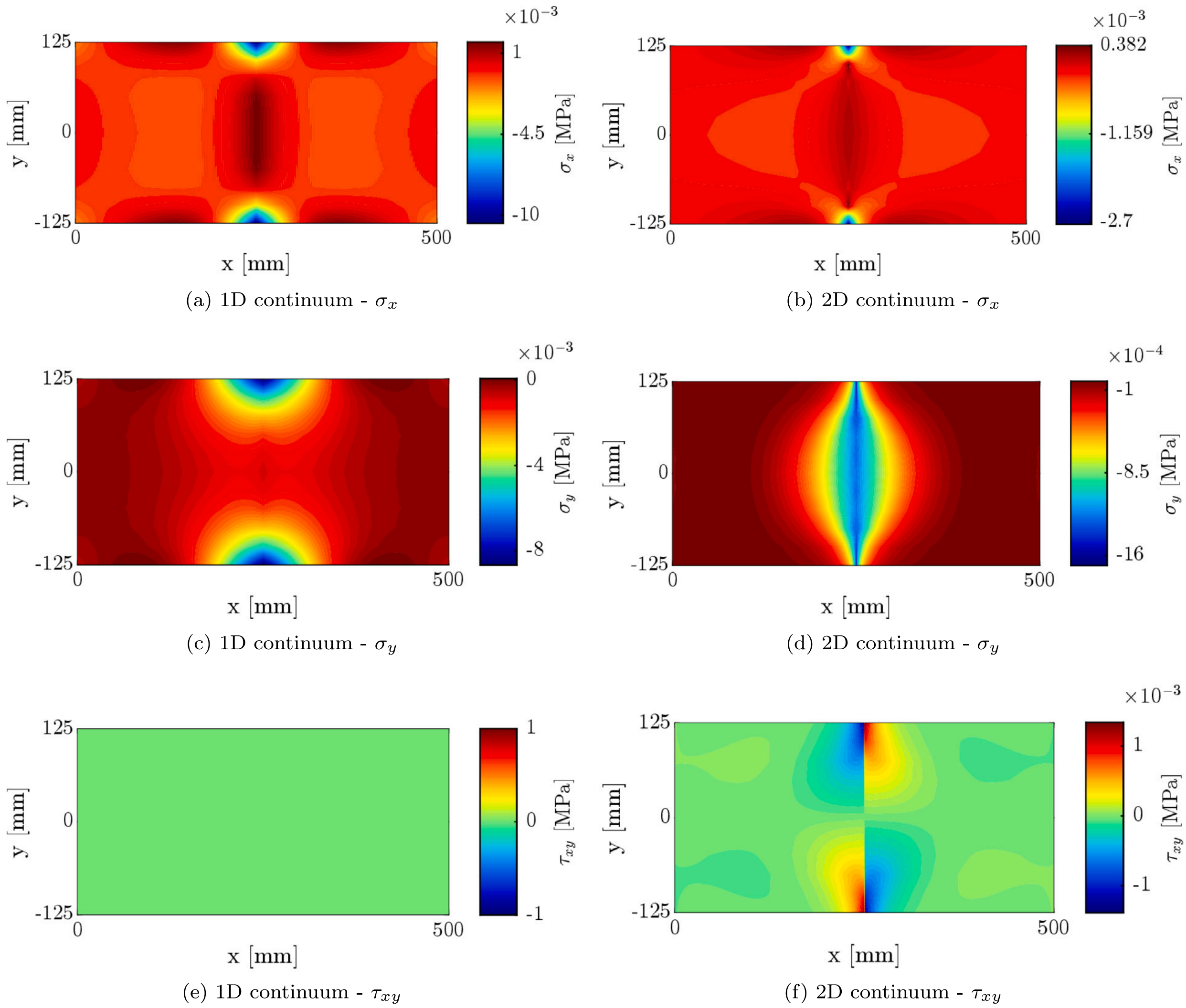

Fig. 14. Stress fields of the transversally loaded FG clamped–clamped beam with a quadratic variation of the Young modulus along the thickness specified in Eq. (58) and subjected to a pair of concentrated forces $\mathscr{F}_\theta$ at midspan. Left column: proposed one-dimensional beam formulation; right column: two-dimensional finite element continuum model.

Table 1
Maximum transverse displacement $|v_{\max}|$ (in absolute value) of FG beams for different boundary conditions (BCs) and power-law indices m. Results from the present formulation are compared with those reported in the literature by Li et al. (2019), Ruocco and Reddy (2023b) and Müsevitoğlu et al. (2025), all based on classical Reddy-type beam theory. Three boundary configurations are considered: cantilever (CF), clamped–clamped (CC) and simply supported (SS) beams.

BCs	Scholars	$m = 0$	$m = 0.2$	$m = 0.5$	$m = 1$	$m = 2$	$m = 5$	$m = 10$
CF	Li et al. (2019)	13.564	–	20.847	27.084	–	41.524	45.797
	Ruocco and Reddy (2023b)	13.564	–	20.847	27.084	–	41.524	45.797
	Müsevitoğlu et al. (2025)	13.566	16.516	20.850	27.088	34.778	41.532	45.806
	Present	13.460	16.215	20.515	26.862	34.476	41.180	45.439
CC	Li et al. (2019)	18.485	–	28.088	36.387	–	57.503	64.162
	Ruocco and Reddy (2023b)	18.454	–	28.089	36.387	–	57.504	64.163
	Müsevitoğlu et al. (2025)	18.451	22.353	28.085	36.382	46.939	57.496	64.152
	Present	18.260	21.903	27.578	35.992	46.420	56.876	63.481
SS	Li et al. (2019)	84.289	–	129.630	168.450	–	257.730	284.010
	Ruocco and Reddy (2023b)	84.289	–	129.640	168.450	–	257.730	284.010
	Müsevitoğlu et al. (2025)	84.282	102.642	129.627	168.440	216.190	257.704	283.985
	Present	84.407	101.717	128.741	168.629	216.418	258.007	284.358

the elastic inertia properties, which are computed by a Taylor series expansion truncated at the 10th order, since the proposed formula in Eq. (33) is valid only for integer values of m.

Despite these differences, the overall displacement trends predicted by the proposed model are in close agreement with the benchmark results across all boundary conditions.

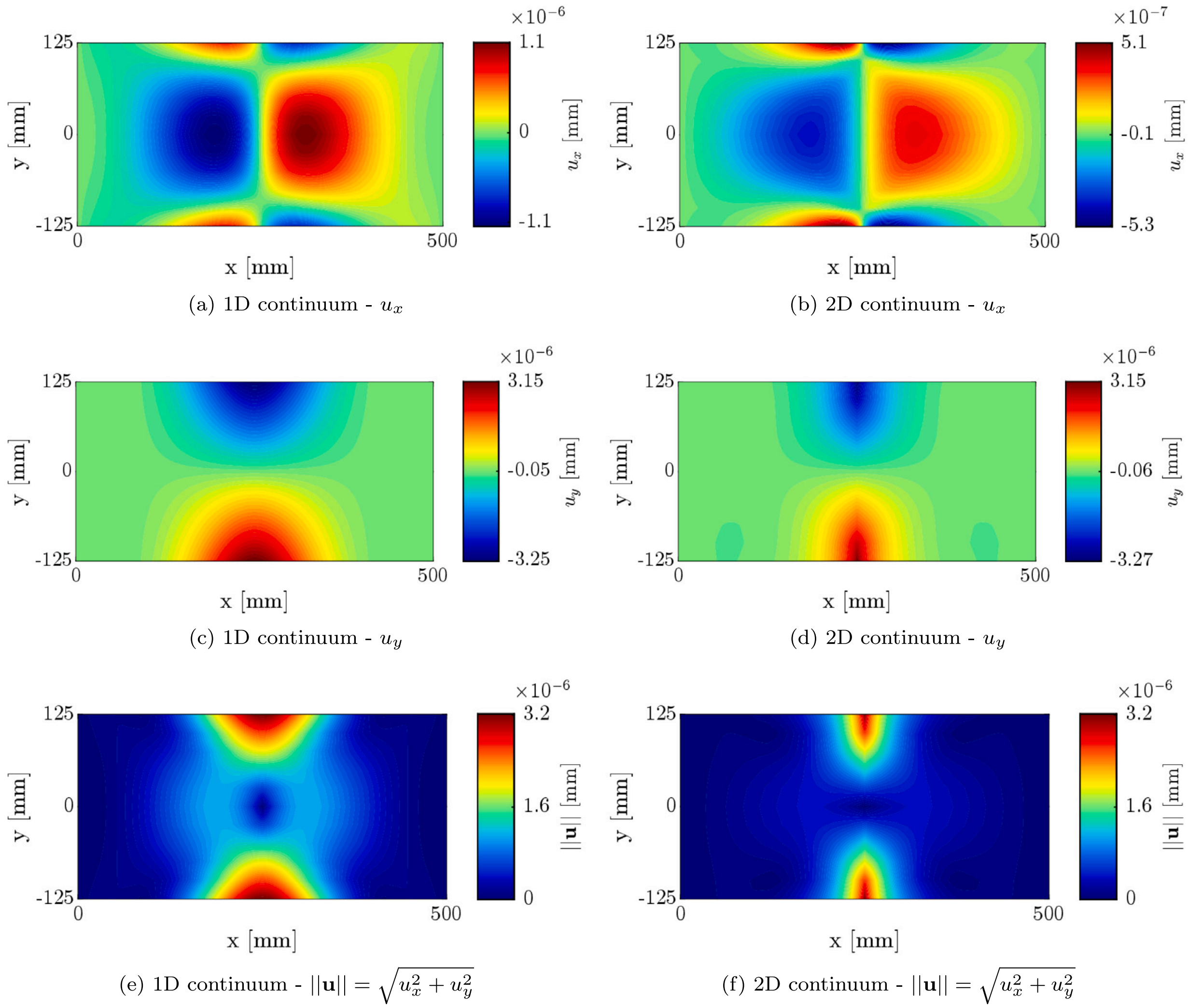

Fig. 15. Displacement fields of the transversally loaded FG clamped–clamped beam with a quadratic variation of the Young modulus along the thickness specified in Eq. (58) and subjected to a pair of concentrated forces $\mathscr{F}_\theta$ at midspan. Left column: proposed one-dimensional beam formulation; right column: two-dimensional finite element continuum model.

These comparisons demonstrate the reliability of the proposed beam model, which accurately reproduces both the global and local mechanical response of FG beams under different loading and boundary conditions.

8. Conclusions

In this paper, a functionally graded enhanced beam model has been developed and investigated. The model extends the classical third-order Reddy theory by including additional kinematic terms, in order to allow for lateral stretching of the beam cross section.

The main findings and original contributions of the present study can be summarised as follows:

- Local equilibrium equations have been derived by a variational method, leading to a consistent and energetically coherent formulation. This allows for the consistent definition of non-standard loading conditions, e.g., dual forces associated with lateral stretch, that cannot be applied to canonical beam theories.
- A constitutive model has been formulated to account for the mechanical behaviour of functionally graded materials (FGMs). Exact analytical formulae have been derived for the local stiffness tensor and its higher-order elastic moments. This provides a general and computationally efficient tool to handle arbitrary polynomial variations of the Young modulus along the beam thickness.
- The finite element method has been employed to discretise the governing equations derived from the variational formulation. One-dimensional two-node elements have been implemented, with shape functions chosen to satisfy the continuity and differentiability requirements imposed by the weak form.
- The predicted stress and strain fields for both linear and nonlinear FGM gradations are consistent with detailed 2D continuum finite element analyses and literature benchmarks, successfully capturing the non-uniform distributions characteristic of functionally graded materials. Additionally, validation against benchmark results from the literature demonstrates that the proposed beam model is accurate and efficient in predicting the static response of FG beams.

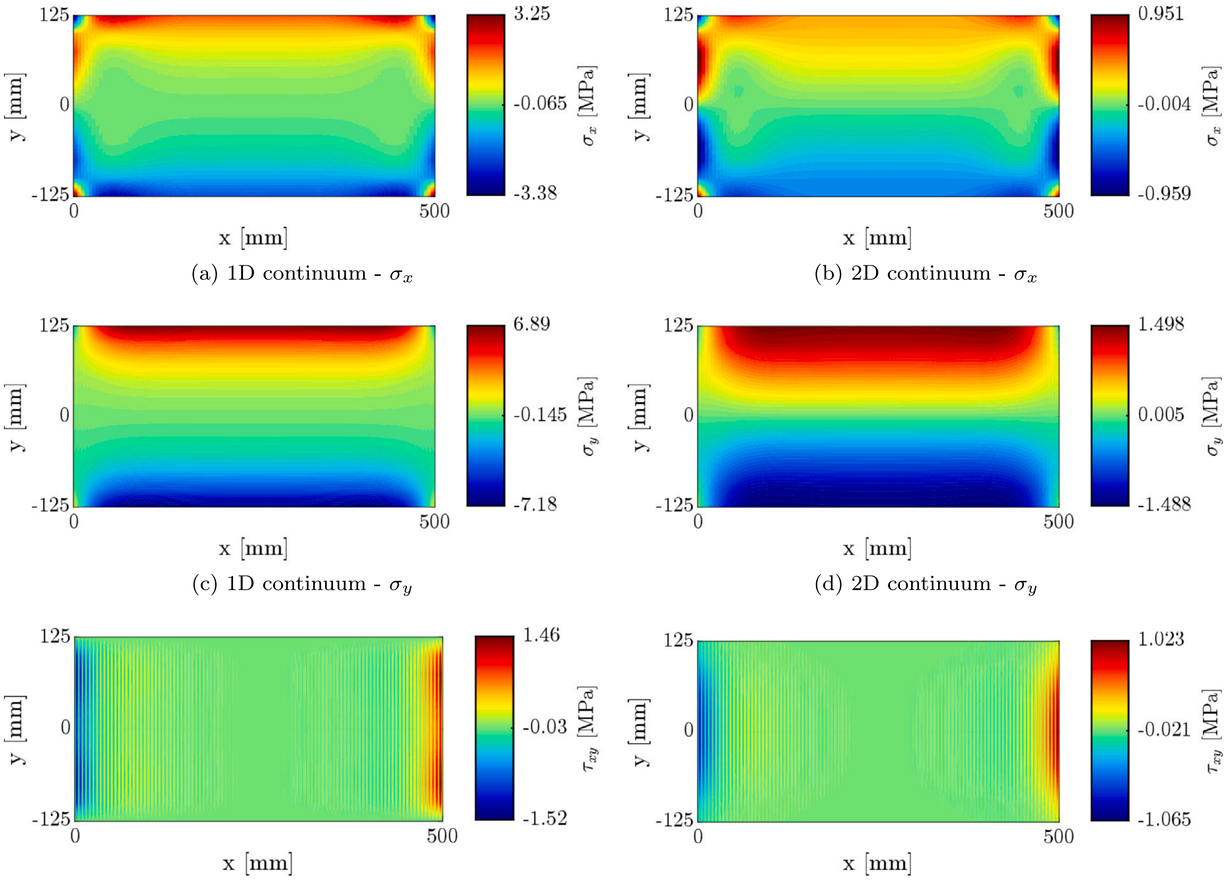

(a) 1D continuum - σ_x (b) 2D continuum - σ_x

(c) 1D continuum - σ_y (d) 2D continuum - σ_y

(e) 1D continuum - τ_{xy} (f) 2D continuum - τ_{xy}

Fig. 16. Stress fields of the transversally loaded FG clamped–clamped beam with a quadratic variation of the Young modulus along the thickness specified in Eq. (58) and subjected to a uniformly distributed load q_ψ. Left column: proposed one-dimensional beam formulation; right column: two-dimensional finite element continuum model.

The general applicability of the proposed model extends far beyond the specific problems investigated herein. Because the governing equations and boundary conditions are derived by a rigorous, variationally consistent energy approach, the model can be seamlessly adapted to any arbitrary constraint configuration. Additionally, the constitutive formulation, which allows for an arbitrary polynomial variation of the material properties, can be directly applied to other complex heterogeneous cross sections, such as sandwich panels, laminated composites or porous structures. Furthermore, the prediction of complex localised stress fields and thickness stretching effects in FG structures represents a main advantage of the proposed model, providing a computationally efficient 1D alternative to expensive full 3D finite element analyses.

Future developments will focus on the implementation of dynamic analyses and stability problems, as well as the integration of the proposed beam model into shell formulations for the analysis of morphing and slender structural elements.

CRediT authorship contribution statement

Davide Pellecchia: Writing – review & editing, Writing – original draft, Visualization, Validation, Software, Methodology, Investigation, Funding acquisition, Formal analysis, Data curation, Conceptualization. **Francesco Marmo:** Writing – review & editing, Validation, Supervision, Software. **Giambattista Romano:** Writing – review & editing, Validation. **Eugenio Ruocco:** Writing – review & editing, Validation, Supervision, Conceptualization.

Declaration of competing interest

The authors declare that they have no known competing financial interests or personal relationships that could have appeared to influence the work reported in this paper.

Acknowledgements

This work was supported by the European Union - Next Generation EU and MUR (Italy) within the projects PNRR 2024 Cultural Heritage Active Innovation for Sustainable Society CHANGES [code PE0000020, University of Naples Federico II Research Unit CUP: E53C22001650006].

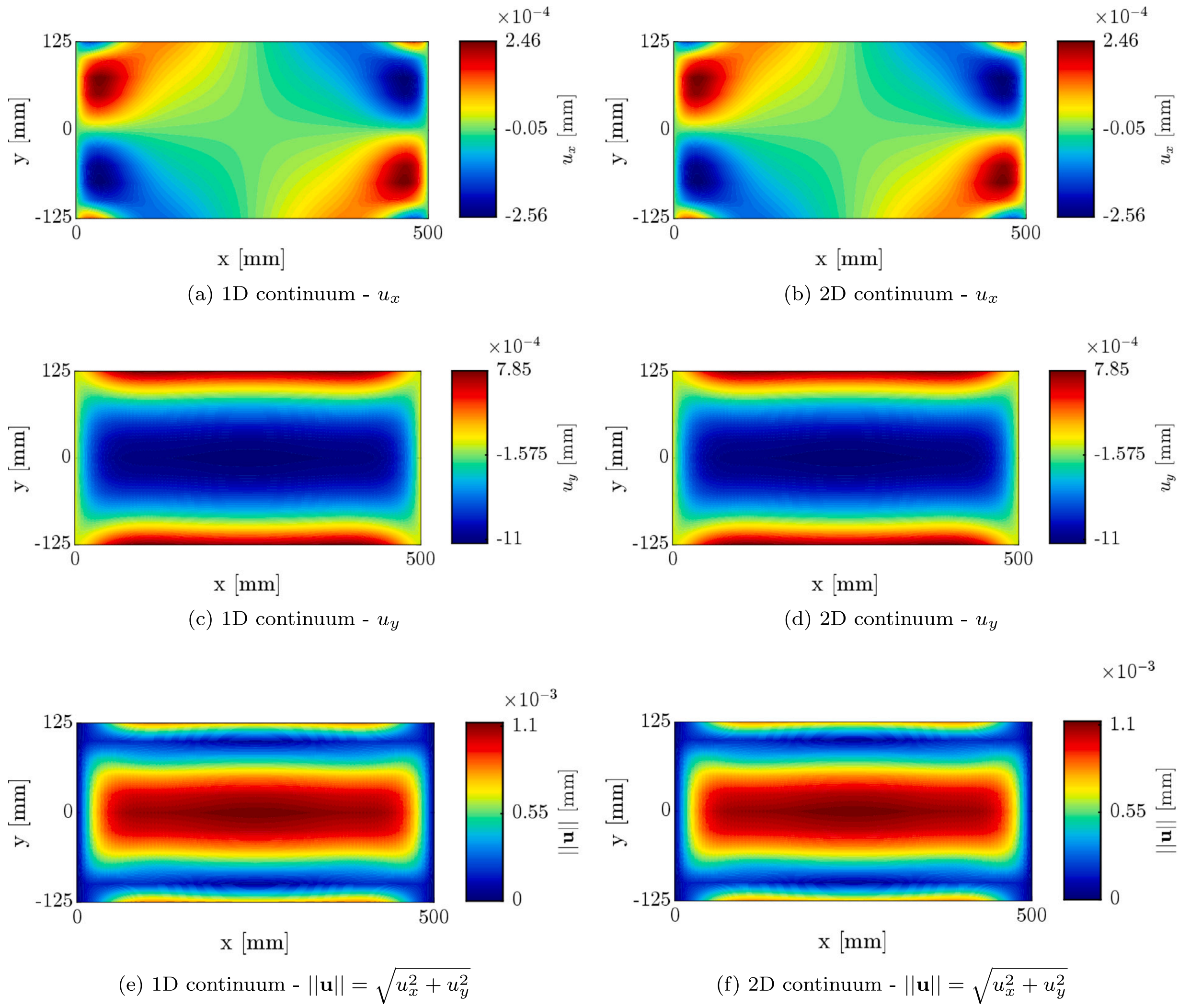

Fig. 17. Displacement fields of the transversally loaded FG clamped–clamped beam with a quadratic variation of the Young modulus along the thickness specified in Eq. (58) and subjected to a uniformly distributed load q_v. Left column: proposed one-dimensional beam formulation; right column: two-dimensional finite element continuum model.

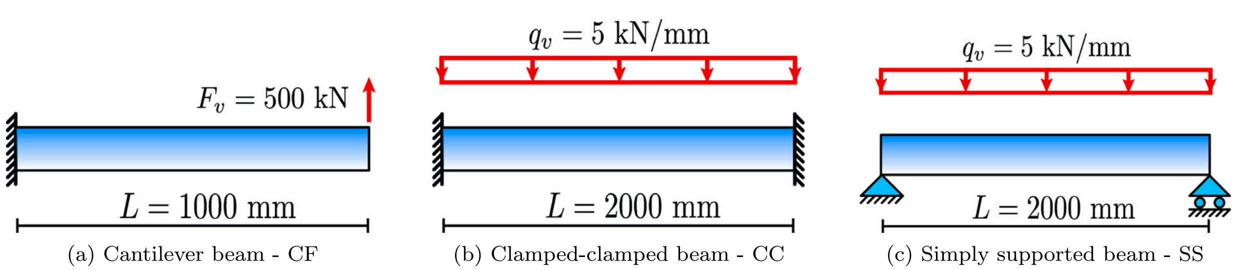

Fig. 18. Geometry, loading and boundary conditions of the FG beams reported in the literature and considered for validation. (a) Cantilever beam (CF); (b) clamped–clamped beam (CC); and (c) simply supported beam (SS).

Data availability

Data will be made available on request.

References

Akavci, S., Tanrikulu, A., 2015. Static and free vibration analysis of functionally graded plates based on a new quasi-3D and 2D shear deformation theories. Composites B 83, 203–215. http://dx.doi.org/10.1016/j.compositesb.2015.08.043.

Aydogdu, M., Taskin, V., 2007. Free vibration analysis of functionally graded beams with simply supported edges. Mater. Des. 28, 1651–1656.

Belabed, Z., Bousahla, A.A., Tounsi, A., 2024a. Vibrational and elastic stability responses of functionally graded carbon nanotube reinforced nanocomposite beams via a new Quasi-3D finite element model. Comput. Concr. 34 (5), 625–648.

Belabed, Z., Tounsi, A., Bousahla, A.A., Tounsi, A., Yaylacı, M., 2024b. Accurate free and forced vibration behavior prediction of functionally graded sandwich beams with variable cross-section: A finite element assessment. Mech. Based Des. Struct. Mach. 52 (11), 9144–9177. http://dx.doi.org/10.1080/15397734.2024.2337914.

Bousmaha, K., Belalia, S.A., Chorfi, S.M., Tounsi, A., Al-Osta, M.A., Alluqmani, A.E., 2025. On the dynamic behavior of plates made of porous advanced materials reinforced with carbon nanotubes using a p-version of finite element method. Mech. Based Des. Struct. Mach. 1–30. http://dx.doi.org/10.1080/15397734.2025.2534679.

Carrera, E., 2003. Theories and finite elements for multilayered plates and shells: a unified compact formulation with numerical assessment and benchmarking. Arch. Comput. Methods Eng. 10 (3), 215–296.

Carrera, E., Brischetto, S., Cinefra, M., Soave, M., 2011. Effects of thickness stretching in functionally graded plates and shells. Composites B 42 (2), 123–133. http://dx.doi.org/10.1016/j.compositesb.2010.10.005.

Chen, X., Li, R., Chang, C., Cheng, L., 2025. 3D dynamic analysis of elastically restrained multi-directional FGMs rectangular parallelepiped. Int. J. Mech. Sci. 287, 109950. http://dx.doi.org/10.1016/j.ijmecsci.2025.109950.

Filippi, M., Carrera, E., Zenkour, A., 2015. Static analyses of FGM beams by various theories and finite elements. Composites B 72, 1–9.

Fu, Y., Chen, Y., Zhang, P., 2013. Thermal buckling analysis of functionally graded beam with longitudinal crack. Meccanica 48, 1227–1237.

Grover, N., Maiti, D., Singh, B., 2013. A new inverse hyperbolic shear deformation theory for static and buckling analysis of laminated composite and sandwich plates. Compos. Struct. 95, 667–675.

Heyliger, P.R., Reddy, J.N., 1988. A higher order beam finite element for bending and vibration problems. J. Sound Vib. 126 (2), 309–326.

Hirai, T., Chen, L., 1999. Recent and prospective development of functionally graded materials in Japan. Mater. Sci. Forum 308, 509–514.

Jin, G., Chen, Y., Li, S., Ye, T., Zhang, C., 2019. Quasi-3D dynamic analysis of rotating FGM beams using a modified Fourier spectral approach. Int. J. Mech. Sci. 163, 105087. http://dx.doi.org/10.1016/j.ijmecsci.2019.105087.

Kadoli, R., Akhtar, K., Ganesan, N., 2008. Static analysis of functionally graded beams using higher order shear deformation theory. Appl. Math. Model. 32, 2509–2525.

Karama, M., Afaq, K., Mistou, S., 2003. Mechanical behaviour of laminated composite beam by the new multi-layered laminated composite structures model with transverse shear stress continuity. Int. J. Solids Struct. 40 (6), 1525–1546.

Lakhdar, Z., Chorfi, S.M., Belalia, S.A., Khedher, K.M., Alluqmani, A.E., Tounsi, A., Yaylacı, M., 2024. Free vibration and bending analysis of porous bi-directional FGM sandwich shell using a TSDT p-version finite element method. Acta Mech. 235 (6), 3657–3686. http://dx.doi.org/10.1007/s00707-024-03909-y.

Lee, J.K., Lee, B.K., 2019. Free vibration and buckling of tapered columns made of axially functionally graded materials. Appl. Math. Model. 75, 73–87. http://dx.doi.org/10.1016/j.apm.2019.05.010.

Li, S.R., Batra, R.C., 2013. Relations between buckling loads of functionally graded Timoshenko and homogeneous Euler–Bernoulli beams. Compos. Struct. 95, 5–9.

Li, S.R., Cao, D.F., Wan, Z.Q., 2013. Bending solutions of FGM Timoshenko beams from those of homogeneous Euler–Bernoulli beams. Appl. Math. Model. 37, 7077–7085.

Li, W., Ma, H., Gao, W., 2019. A higher-order shear deformable mixed beam element model for accurate analysis of functionally graded sandwich beams. Compos. Struct. 221, 110830. http://dx.doi.org/10.1016/j.compstruct.2019.04.002.

Liu, W., Zhang, Z., Xin, L., Li, Z., 2025. A multiscale finite element analysis model for functionally graded graphene reinforced composites considering graphene defects. Compos. Struct. 371, 119499.

Love, A.E.H., 2013. A Treatise on the Mathematical Theory of Elasticity. Cambridge Univ Press.

Mahi, A., Bedia, E.A.A., Tounsi, A., 2015. A new hyperbolic shear deformation theory for bending and free vibration analysis of isotropic, functionally graded, sandwich and laminated composite plates. Appl. Math. Model. 39 (9), 2489–2508.

Mahi, A., Bedia, E.A.A., Tounsi, A., Mechab, I., 2010. An analytical method for temperature-dependent free vibration analysis of functionally graded beams with general boundary conditions. Compos. Struct. 92, 1877–1887.

Mantari, J.L., Oktem, A.S., Soares, C.G., 2012. A new trigonometric shear deformation theory for isotropic, laminated composite and sandwich plates. Int. J. Solids Struct. 49 (1), 43–53.

Meftah, S.A., Aldosari, S.M., Tounsi, A., Cuong-Le, T., Khedher, K.M., Alluqmani, A.E., 2024. Simplified homogenization technique for nonlinear finite element analysis of in-plane loaded masonry walls. Eng. Struct. 306, 117822. http://dx.doi.org/10.1016/j.engstruct.2024.117822.

Murin, J., Aminbaghai, M., Kutis, V.T., 2010. Exact solution of the bending vibration problem of FGM beams with variation of material properties. Eng. Struct. 32, 1631–1640.

Müsevitoğlu, A., Özütok, A., Reddy, J.N., 2025. Static analysis of functionally graded and laminated composite beams using various higher-order shear deformation theories: A study with mixed finite element models. Eur. J. Mech. A Solids 111, 105596. http://dx.doi.org/10.1016/j.euromechsol.2025.105596.

Nguyen, V.H., Nguyen, T.K., Thai, H.T., Vo, T.P., 2014. A new inverse trigonometric shear deformation theory for isotropic and functionally graded sandwich plates. Composites B 66, 233–246.

Pellecchia, D., Vaiana, N., Sessa, S., Castellano, A., 2024. Mass moments of functionally graded 2D domains and axisymmetric solids. Appl. Math. Model. 129, 250–274. http://dx.doi.org/10.1016/j.apm.2024.01.028.

Pradhan, K.K., Chakraverty, S., 2013. Free vibration of Euler and Timoshenko functionally graded beams by the Rayleigh–Ritz method. Composites B 51, 175–184.

Reddy, J.N., 1984. A simple higher order theory for laminated composite plates. Trans. ASME, J. Appl. Mech. 51 (4), 745–752.

Reddy, J.N., 2017. Energy Principles and Variational Methods in Applied Mechanics, third ed. Wiley.

Reddy, J.N., 2022. Theories and Analyses of Beams and Axisymmetric Circular Plates. Taylor & Francis.

Ruocco, E., Forooghi, A., Pellecchia, D., Marmo, F., Rosati, L., 2025. An improved Reddy beam model accounting for Poisson effect. Mech. Adv. Mater. Struct. 1–17. http://dx.doi.org/10.1080/15376494.2025.2512460.

Ruocco, E., Reddy, J.N., 2022. A new nonlinear 5-parameter beam model accounting for the Poisson effect. Int. J. Non Linear Mech. 142, 103996.

Ruocco, E., Reddy, J.N., 2023a. Analytical solutions of Reddy, Timoshenko and Bernoulli beam models: A comparative analysis. Eur. J. Mech. A-Solid 99, 104953. http://dx.doi.org/10.1016/j.euromechsol.2023.104953.

Ruocco, E., Reddy, J.N., 2023b. A closed-form solution for accurate stress analysis of functionally graded Reddy beams. Compos. Struct. 307, 116676. http://dx.doi.org/10.1016/j.compstruct.2023.116676.

Ruocco, E., Reddy, J.N., Sacco, E., 2021. Analytical solution for a 5-parameter beam displacement model. Int. J. Mech. Sci. 201, 106496.

Shao, D., Gao, M., Wu, D., Sun, N., 2025. A unified dynamic modeling for FGM sandwich conical shell built-in reinforcing plate in airflow environment. Aerosp. Sci. Technol. 162, 110204.

Shen, H.S., 2009. Functionally Graded Materials Nonlinear Analysis of Plates and Shells. CRC Press, Boca Raton.

Shen, H.-S., Wang, Z.-X., 2014. Nonlinear analysis of shear deformable FGM beams resting on elastic foundations in thermal environments. Int. J. Mech. Sci. 81, 195–206. http://dx.doi.org/10.1016/j.ijmecsci.2014.02.020.

Simsek, M., 2010. Fundamental frequency analysis of functionally graded beams by using different higher-order beam theories. Nucl. Eng. Des. 240, 697–705.

Soldatos, K., 1992. A transverse shear deformation theory for homogeneous monoclinic plates. Acta Mech. 94 (3–4), 195–220.

Thai, H.-T., Kim, S.-E., 2013. A simple quasi-3D sinusoidal shear deformation theory for functionally graded plates. Compos. Struct. 99, 172–180. http://dx.doi.org/10.1016/j.compstruct.2012.11.030.

Tounsi, A., Belabed, Z., Bounouara, F., Balubaid, M., Mahmoud, S.R., Bousahla, A.A., Tounsi, A., 2026. A finite element approach for forced dynamical responses of porous FG nanocomposite beams resting on viscoelastic foundations. Int. J. Struct. Stab. Dyn. 26 (11), 2650078. http://dx.doi.org/10.1142/S0219455426500781.

Touratier, M., 1991. An efficient standard plate theory. Internat. J. Engrg. Sci. 28 (3), 901–916.

Vaccaro, M.S., Barretta, R., Marotti de Sciarra, F., Reddy, J.N., 2022. Nonlocal integral elasticity for third-order small-scale beams. Acta Mechanica 233 (6), 2393–2403. http://dx.doi.org/10.1007/s00707-022-03210-w.

Van Huong, N., Cong, P.H., Duc, N.D., 2025. Nonlinear buckling and vibration of electromagnetic sandwich plates with graphene-origami-reinforced copper matrix layers and a functionally graded porous core in thermal environment. Aerosp. Sci. Technol. 166, 110596.

Vo, T.P., Thai, H.-T., Nguyen, T.-K., Inam, F., Lee, J., 2015. A quasi-3D theory for vibration and buckling of functionally graded sandwich beams. Compos. Struct. 119, 1–12. http://dx.doi.org/10.1016/j.compstruct.2014.08.006.

Wakashima, K., Hirano, T., Niino, M., 1990. Space applications of advanced structural materials. In: ESA SP-303. European Space Agency, p. 97.

Woodward, B., Kashtalyan, M., 2012. Performance of functionally graded plates under localised transverse loading. Compos. Struct. 94, 2254–2262.

Ying, J., Lu, C.F., Chen, W.Q., 2008. Two-dimensional elasticity solutions for functionally graded beams resting on elastic foundations. Compos. Struct. 84, 209–219.

Youzera, H., Meftah, S.A., Tounsi, A., Ghazwani, M.H., Alnujaie, A., 2025. Finite element formulation for free vibration analysis of porous FGM beams under thermal excitation. Comput. Concr. 36 (4), 419–430. http://dx.doi.org/10.12989/cac.2025.36.4.419.

Zhang, S., Yin, X., Zhao, J., Tian, L., Guan, S., Tian, J., 2025. Bamboo-inspired functionally graded aluminum foams: Significantly enhanced mechanical and thermal insulation properties. Constr. Build. Mater. 491, 142697.

Zhang, Q., Yuan, Y., 2025. Effect of projectile nose shape on ballistic resistance of multi-layered explosively welded plates. Int. J. Impact Eng. 196, 105151.

Zienkiewicz, O.C., Taylor, R.L., 2000a. Finite Element Method: Volume 1 - The Basis, fifth ed. Butterworth-Heinemann, Oxford.

Zienkiewicz, O.C., Taylor, R.L., 2000b. The Finite Element Method: Volume 2 - Solid Mechanics, fifth ed. Butterworth-Heinemann, Oxford.